AFRL-RX-WP-TR-2019-0163

INFLUENCE OF TEST METODOLOGY AND ENVIRONMENT ON STRESS RUPTURE LIFE OF NEXTEL720/AS

Larry P. Zawada
Universal Technology Corporation (UTC)

Craig Przybyla
AFRL/RXCC

Jennifer L. Pierce
University Of Dayton Research Institute (UDRI)

30 APRIL 2019
Final Report

DISTRIBUTION STATEMENT A.
Approved for public release: Distribution is unlimited.

AIR FORCE RESEARCH LABORATORY
MATERIALS AND MANUFACTURING DIRECTORATE
WRIGHT-PATTERSON AIR FORCE BASE, OH 45433-7750
AIR FORCE MATERIEL COMMAND
UNITED STATES AIR FORCE

NOTICE AND SIGNATURE PAGE

Using Government drawings, specifications, or other data included in this document for any purpose other than Government procurement does not in any way obligate the U.S. Government. The fact that the Government formulated or supplied the drawings, specifications, or other data does not license the holder or any other person or corporation; or convey any rights or permission to manufacture, use, or sell any patented invention that may relate to them.

This report was cleared for public release by the USAF 88th Air Base Wing (88 ABW) Public Affairs Office (PAO) and is available to the general public, including foreign nationals.

Copies may be obtained from the Defense Technical Information Center (DTIC) (http://www.dtic.mil).

AFRL-RX-WP-TR-2019-0163 HAS BEEN REVIEWED AND IS APPROVED FOR PUBLICATION IN ACCORDANCE WITH ASSIGNED DISTRIBUTION STATEMENT.

_____//signature//_____
JEFF BAUR
Project Engineer
Composite Branch
Structural Materials Division

_____//signature//_____
JENNIFER FIELDING
Section Chief
Composite Branch
Structural Materials Division

_____//signature//_____
AMBER DAVIS
Deputy Division Chief
Structural Materials Division
Materials And Manufacturing Directorate

This report is published in the interest of scientific and technical information exchange, and its publication does not constitute the Government's approval or disapproval of its ideas or findings.

REPORT DOCUMENTATION PAGE

Form Approved
OMB No. 0704-0188

The public reporting burden for this collection of information is estimated to average 1 hour per response, including the time for reviewing instructions, searching existing data sources, searching existing data sources, gathering and maintaining the data needed, and completing and reviewing the collection of information. Send comments regarding this burden estimate or any other aspect of this collection of information, including suggestions for reducing this burden, to Department of Defense, Washington Headquarters Services, Directorate for Information Operations and Reports (0704-0188), 1215 Jefferson Davis Highway, Suite 1204, Arlington, VA 22202-4302. Respondents should be aware that notwithstanding any other provision of law, no person shall be subject to any penalty for failing to comply with a collection of information if it does not display a currently valid OMB control number. **PLEASE DO NOT RETURN YOUR FORM TO THE ABOVE ADDRESS**.

1. REPORT DATE *(DD-MM-YY)*	2. REPORT TYPE	3. DATES COVERED *(From - To)*
30 April 2019	Final	21 January 2010 – 5 January 2015

4. TITLE AND SUBTITLE
INFLUENCE OF TEST METHODOLOGY AND ENVIRONMENT ON STRESS RUPTURE LIFE OF NEXTEL720/AS

5a. CONTRACT NUMBER
In-House

5b. GRANT NUMBER

5c. PROGRAM ELEMENT NUMBER
62102F

6. AUTHOR(S)
Craig Przybyla – AFRL/RXCC
Larry P. Zawada – UTC
Jennifer L. Pierce – UDRI

5d. PROJECT NUMBER
4347

5e. TASK NUMBER

5f. WORK UNIT NUMBER
X0S7

7. PERFORMING ORGANIZATION NAME(S) AND ADDRESS(ES)
AFRL/RXCC and AFRL/RXCM
Composites Branch; Structural Materials Division
Materials and Manufacturing Directorate
2230 Tenth Street, Suite 1
Wright Patterson Air Force Base, OH 45433 (see back)

8. PERFORMING ORGANIZATION REPORT NUMBER
AFRL-RX-WP-TR-2019-0163

9. SPONSORING/MONITORING AGENCY NAME(S) AND ADDRESS(ES)
Air Force Research Laboratory
Materials and Manufacturing Directorate
Wright-Patterson Air Force Base, OH 45433-7750
Air Force Materiel Command
United States Air Force

10. SPONSORING/MONITORING AGENCY ACRONYM(S)
AFRL/RXCC

11. SPONSORING/MONITORING AGENCY REPORT NUMBER(S)
AFRL-RX-WP-TR-2019-0163

12. DISTRIBUTION/AVAILABILITY STATEMENT
DISTRIBUTION STATEMENT A. Approved for public release: distribution is unlimited.

13. SUPPLEMENTARY NOTES:
PA Case Number: 88ABW-2019-2847; Clearance Date: 07 Jun 2019. Report contains color.

14. ABSTRACT (*Maximum 200 words*):
A dedicated experimental test program was conducted to study how testing issues, test specimen geometry, and environmental issues affect the variability in stress rupture life of an oxide-oxide ceramic matrix composite (N720/AS). This report identifies several factors that contributed to the variability in measured stress rupture life.

15. SUBJECT TERMS
ceramic matrix composites, stress rupture, thermal protection systems, high temperature, probability of failure

16. SECURITY CLASSIFICATION OF:			17. LIMITATION OF ABSTRACT:	18. NUMBER OF PAGES	19a. NAME OF RESPONSIBLE PERSON (Monitor)
a. REPORT	b. ABSTRACT	c. THIS PAGE	SAR	58	Jeff Baur
Unclassified	Unclassified	Unclassified			19b. TELEPHONE NUMBER *(Include Area Code)* (937) 255-3622

REPORT DOCUMENTATION PAGE Cont'd

6. AUTHOR(S)

Craig Przybyla – AFRL/RXCC
Larry P. Zawada – UTC
Jennifer L. Pierce – UDRI

7. PERFORMING ORGANIZATION NAME(S) AND ADDRESS(ES)

Universal Technology Corporation (UTC)
1270 North Fairfield Road
Dayton, Ohio 45432-2600

University of Dayton Research Institute (UDRI)
Advanced Materials Characterization Group
Structural Integrity Division
300 College Park
Dayton, OH 45469-0120

TABLE OF CONTENTS

Section **Page**

LIST OF FIGURES ii
LIST OF TABLES iv
ABSTRACT v
1. SUMMARY 1
2. INTRODUCTION 2
   2.1 Program Objectives 2
   2.2 Test Plan 2
   2.3 Literature Review of Variability in CMCs 3
3 MATERIALS DESCRIPTION 6
   3.1 Description of N720/AS 6
   3.2 Processing Of N720/AS 6
   3.3 Microstructure Studies of N720/AS 7
4. TESTING PROCEDURE 14
   4.1 Test Specimen Geometry 14
   4.2 Test Frame and Grips 15
   4.3 Test Frame Alignment 16
   4.4 Furnace and Thermal Profiling 17
   4.5 Testing Procedure for Tension Testing 21
   4.6 Test Procedure for Stress Rupture Testing 22
5. TEST RESULTS 23
   5.1 Tensile Results 23
   5.2 Stress Rupture Results 24
6. DISCUSSION 26
   6.1 Stress Versus Time to Failure 26
   6.2 Probability of Failure 29
   6.3 Humidity Effects 30
   6.4 Failure Location for Each Test Specimen 34
   6.5 Test Specimen Dimensions 36
   6.6 Test Specimen Design 40
   6.7 Effect of Cut Fibers at the Radius 44
7. CONCLUSIONS AND RECOMMENDATIONS 46
8. REFERENCES 47
LIST OF SYMBOLS, ABBREVIATIONS, and ACRONYMS 49

DISTRIBUTION STATEMENT A. Approved for public release: distribution is unlimited.
88ABW-2019-2847

LIST OF FIGURES

Figure **Page**

Figure 1. Plot of Stress versus Time to Failure for N720/AS 3
Figure 2. Ultimate Tensile Strength of Syrlamic 200 by Panel 4
Figure 3. Stress Versus Cycles for SiC/SiC Tested at 23°C [3] 5
Figure 4. Schematic of Processing Methodology Used to Make N720/AS 6
Figure 5. Photo of Tested N720/AS Specimen and Location of Cuts Made for Microstructural Studies 7
Figure 6. Low-Magnification 0/90 Micrograph of Entire Cross Section of N720/AS Test Specimen (100×, B) 8
Figure 7. Low-Magnification 0/90 Micrograph of Entire Cross Section of N720/AS Test Specimen (100×, E) 8
Figure 8. Representative 0/90 Micrograph of N720/AS Microstructure (200×, B) 9
Figure 9. Representative 0/90 Micrograph of N720/AS Microstructure (500×, B) 9
Figure 10. Representative 0/90 Micrograph of N720/AS Microstructure (1000×) 10
Figure 12. Representative ±45 Micrograph of N720/AS Microstructure (200×, C) 11
Figure 13. Representative ±45 Micrograph of N720/AS Microstructure (500×, C) 12
Figure 14. Representative ±45 Micrograph of N720/AS Microstructure (1000×, C) 12
Figure 15. High-Resolution SEM Image of N720 Fibers and Porous Alumino-Silicate Matrix (6000×) 13
Figure 16. Schematic Diagram of Dogbone Test Specimen Geometry Used for N720/AS Stress Rupture Variability Study 15
Figure 17. Photograph of Test System (SH#12) Used for Stress Rupture Testing 16
Figure 18. Straight-Sided Steel Bar Alignment Specimen with Eight Strain Gages 16
Figure 19. Plot of Percent Bending Versus Average Axial Strain 17
Figure 20. Side View of Amteco Furnace Showing Custom-Built Gripping System Developed for Flat CMC Specimens 18
Figure 21. Schematic Showing Placement of Thermocouples for Thermal Profiling 19
Figure 22. Furnace Setup for Thermal Profile of N720/AS Test Specimen Using 11 Thermocouples 19
Figure 23. Photograph of N720/AS Test Specimen Instrumented with Thermocouples for Temperature Profiling 20
Figure 24. Photograph of Test Setup Showing N720/AS Test Specimen with Three Probe Thermocouples in Place 20
Figure 25. Photograph of Furnace Packed with Custom-Cut Insulation 20
Figure 26. Thermal Profile of N720/AS Test Specimen at 1100°C 21
Figure 27. Tensile Stress-Versus-Strain Behavior for N720/AS at 1100°C 24
Figure 28. Stress Versus Linear Time to Failure for N720/AS 26
Figure 29. Stress Versus Log Time to Failure (Hours) for N720/AS 27
Figure 30. Stress Versus Log Time to Failure (Seconds) for N720/AS 27
Figure 31. Stress Versus Time to Failure for Three Panels of N720/AS 28
Figure 32. Stress Versus Time to Failure for Individual Panels of N720/AS 28
Figure 33. Histogram Plot of Time to Failure for N720/AS Showing Bi-Modal Distribution 29
Figure 34. Probability of Failure Versus Time to Failure for N720/AS 30

DISTRIBUTION STATEMENT A. Approved for public release: distribution is unlimited.
88ABW-2019-2847

Figure 35. Probability of Failure Versus Time to Failure for Three Individual Panels of N720/AS 30
Figure 36. Plot of Laboratory Relative Humidity Versus Time 32
Figure 37. Average Laboratory Humidity Versus Time to Failure for N720/AS Stress Rupture Tested at 175 MPa and 1100°C 32
Figure 38. Humidity Versus Log Time to Failure Showing Two Groups of Data 33
Figure 39. POF Plot for N720/AS for Average Humidity Above and Below 35% 33
Figure 40. POF Plot Comparing Entire Data Set To Humidity Data Sets 34
Figure 41. Failure Location Versus Time to Failure for N720/AS Stress Rupture Tested at 175 MPa And 1100°C 36
Figure 42. Photograph of Failed Stress Rupture Specimen That Ran ~70 Hours 36
Figure 43. Photograph of Failed Stress Rupture Specimen That Ran ~111 Hours 36
Figure 44. Average Specimen Thickness Versus Rupture Time for N720/AS 37
Figure 45. Applied Load Versus Rupture Time for N720/AS 38
Figure 46. Average Test Specimen Thickness Along Length of Specimens 40
Figure 47. Stress Contour Plot with ±2% Variation from Applied 100 MPa Net Section Stress for Standard Test Specimen 42
Figure 48. Maximum Localized Stress Value Along Length of Standard Test Specimen 42
Figure 49. Schematic of New Dogbone Test Specimen Geometry for Future Variability Studies 43
Figure 50. Stress Contour Plot with ±2% Variation from Applied 100 MPa Net Section Stress for Revised Test Specimen 43
Figure 51. Stress Versus Distance from Specimen Center to Edge at End of Uniform Gage Section 44
Figure 52. Stress Versus Distance from Specimen Center to Edge at Location of Maximum Stress (29 mm from Center) 44

DISTRIBUTION STATEMENT A. Approved for public release: distribution is unlimited.
88ABW-2019-2847

LIST OF TABLES

Table **Page**

Table 1. Summary of Round-Robin Tensile Data for Nicalon-Sylramic S-200 CFCC [2] 4
Table 2. Dimension Data for Nicalon-Sylramic Tensile Bars from the Testing Labs [2] 4
Table 3. Fiber Volume Fractions and Density of N720/AS Panels 13
Table 4. Temperature Measurements from All Thermocouples Used for 1100°C Thermal Profile of N720/AS Test Specimen 21
Table 5. Tabulated Tensile Results for N720/AS Tested at Room Temperature 23
Table 6. Tabulated Tensile Results for N720/AS Tested at 1100°C 23
Table 7. Stress Rupture Testing Results of N720/AS at 1100°C..... 25
Table 8. Test Specimen and Relative Humidity for N720AS Stress Rupture Tests..... 31
Table 9. Location of Failure for N720/AS Stress Rupture Specimens 35
Table 10. Thickness of Test Specimens Along Gage Length 39
Table 11. Stress Concentration Factors for Several Different CMC Dogbone-Shaped Specimens 43

DISTRIBUTION STATEMENT A. Approved for public release: distribution is unlimited.
88ABW-2019-2847

ABSTRACT

A dedicated experimental test program was conducted to study how testing issues, test specimen geometry, and environmental issues affect the variability in stress rupture life of an oxide-oxide ceramic matrix composite (N720/AS). This report identifies several factors that contributed to the variability in measured stress rupture life. The work described in this report was performed by the Composite Performance Research Team of the Composites Branch, Structural Materials Division of the Materials & Manufacturing Directorate, Air Force Research Laboratory (AFRL/RXCC). Larry P. Zawada was the principal investigator and program manager. This report describes the results of a study focused on identification of testing variables, test specimen geometry, and environmental effects on variability in stress rupture life of an oxide/oxide ceramic-matrix composite (CMC).

DISTRIBUTION STATEMENT A. Approved for public release: distribution is unlimited.
88ABW-2019-2847

1. SUMMARY

USAF researchers (AFRL/RXCC) conducted an in-house research program focused on evaluating the factors that influence variability in lifetimes of Ceramic Matrix Composites (CMC) tested at high-temperatures. The goal was the identification of specific contributors to observed variability, such that this information can be shared with the entire CMC community. Establishment of this knowledge base will provide a better understanding of the behavior and life-limiting mechanisms of high-temperature CMCs. Such information is required for materials technology maturation and behavior modeling. The material selected for this study was an oxide/oxide system made by COI Ceramics, Inc. (COIC)[1]. The composite consisted of Nextel™ 720 fibers in an alumino-silicate matrix. This report focuses on testing variables, test specimen geometry, and environmental effects on the measured stress rupture behavior of N720/AS.

[1] COI Ceramics, Inc. is an ATK Space affiliate, 9617 Distribution Avenue, San Diego, CA 92121.

DISTRIBUTION STATEMENT A. Approved for public release: distribution is unlimited.
88ABW-2019-2847

2. INTRODUCTION

AFRL is leading critical science and technology efforts to develop CMCs, and has many different activities focused on establishing a comprehensive knowledge base for these advanced material systems. A segment of this work has involved an AFRL Materials & Manufacturing Directorate (RXCCP) in-house research program focused on evaluating the high-temperature performance of oxide/oxide CMCs under static loading.

2.1 Program Objectives

This report focuses on identification of issues that contribute to variability in stress rupture life of N720/AS.

The specific technical objectives of this investigation were to:

1) Assess issues that influence variability in stress rupture life of N270/AS:
   a. Documentation of failure times for different panels
   b. Establishing sensitivity to test parameters
   c. Evaluation of environmental effects
   d. Documentation of test specimen dimensional effects
   e. Documentation of test specimen geometry effects

2.2 Test Plan

The test plan focused on tensile and stress rupture behavior using three panels of N720/AS. In-plane tensile tests were performed to generate the basic tensile properties such as modulus (E), ultimate tensile strength (UTS), proportional limit (PL), and strain at failure (ε_f), as well as documenting the stress-versus-strain behavior. A substantial number of stress rupture tests were to be conducted to establish variability in life for each CMC panel and the entire data set. Tests were to be performed without high-resolution contact strain measurement to avoid any influence in life from the extensometer rods contacting the specimen. Testing would be conducted at only 1100°C and one stress level that was selected after studying earlier creep rupture testing results [1] that were conducted to determine the run-out stress at 1100°C for 100 hours and additional in-house testing for a 20-hour life (see Figure 1). From the data, it was estimated that testing at 175 MPa would produce failures in approximately 50 to100 hours. The thought was that this limit would produce a valuable data set that would provide excellent confidence for short- and medium-term applications by identifying the spread in time to failure and testing parameters that influence the measured lifetimes.

DISTRIBUTION STATEMENT A. Approved for public release: distribution is unlimited.
88ABW-2019-2847

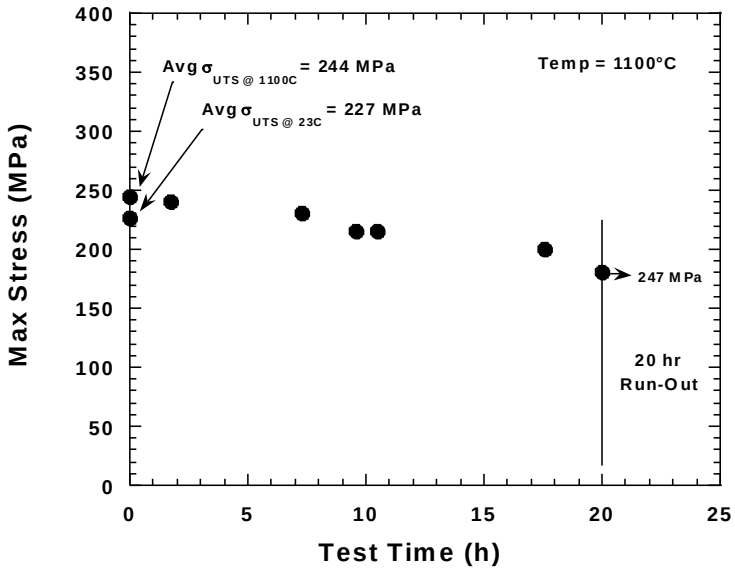

Figure 1. Plot of Stress versus Time to Failure for N720/AS

2.3 Literature Review of Variability in CMCs

For many years, the CMC community has been interested in the topic of variability in CMCs. However, very few studies have been conducted to address this issue for several reasons. Throughout the years, the pedigree of almost all of the current CMCs changed as manufacturers sought to improve the high-temperature performance of their composite systems. As a result, very few were interested in testing a large number of specimens on a system that might not be around in one year. Both the very high cost of current CMCs and testing them at elevated temperatures above 1000°C also contributed to very few repeat tests. For these reasons, most test data in the literature was limited to approximately three repeats per test condition. However, there are a few cases where a larger number of repeat tests were conducted, two of which will be presented below.

The American Society for Testing and Materials (ASTM) conducted a round-robin study focused on tension testing Nicalon/SiC (silicon carbide) at room temperature to determine statistics for the room-temperature tension testing standard that had recently been approved. The study was conducted by Steve Gonczy [2] and documented the results from 9 laboratories that each tension tested 10 specimens. This is an excellent source of data on issues associated with variation in room-temperature test results for a SiC/SiC composite. Several findings of this study were applied to this investigation.

The ASTM study found that the UTS was 251.1 MPa with a mean of ±18 MPa. The coefficient of variation was calculated to be 7.2%. These results indicate some variation in this CMC, but a variation of only ±7% in UTS is relatively minor and indicates that, for room-temperature tensile results, excessive scatter was not observed. It is worth noting that 58 specimens failed in the machined 35 mm gage length (in-gage failure), while 35 specimens were noted to have failed at or outside the start of the radius (out-of-gage failure). The measured mean strength was 251.4

DISTRIBUTION STATEMENT A. Approved for public release: distribution is unlimited.
88ABW-2019-2847

MPa for in-gage failures and 250.5 MPa for out-of-gage failures, showing no statistical difference between these types of failures. Three panels were used to manufacture the 90 test specimens. Results of UTS versus panel are presented in Figure 2 and clearly show a statistical difference between Panels 12, 14, and 16.

Table 1. Summary of Round-Robin Tensile Data for Nicalon-Sylramic S-200 CFCC [2]

	Ultimate Tensile Load	Ultimate Tensile Strength	Ultimate Tensile Strain	Elastic Modulus
Grand Mean*	5570 N	251.1MPa	43.10%	93.0 GPa
Grand Standard Deviation*	367.1 N	18.0 MPa	3.90%	4.65 GPa
Grand Coefficient of Variation*	6.60%	7.20%	9.10%	5.00%
Total Specimen Count	90	90	89	90

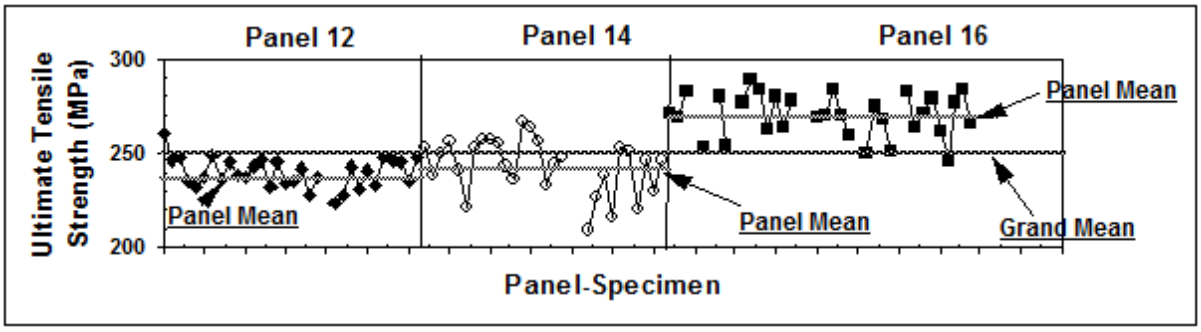

Figure 2. Ultimate Tensile Strength of Syrlamic 200 by Panel [2]

The ASTM study also considered measurements made on the test specimens, with results presented in **Error! Reference source not found.**. There was very little variation in the width, as the edges had been diamond ground, but thickness measurements exhibited a spread in values of approximately 2.5%, indicating that attention needs to be paid to how the specimen dimensions are measured.

Table 2. Dimension Data for Nicalon-Sylramic Tensile Bars from the Testing Labs [2]

DISTRIBUTION STATEMENT A. Approved for public release: distribution is unlimited.
88ABW-2019-2847

Dimension	Gage Thickness (mm)	Gage Width (mm)	Gage X-Section (mm^2)
Grand Mean	2.77	8.01	22.2
Std. Dev.	0.07	0.08	0.63
C. of Variation	2.50%	1.00%	2.90%
Max	2.95	8.16	23.49
Min	2.61	7.58	20.37
Count	90	90	90

In another study performed by Reynaud [3], a SiC/SiC CMC was tested in fatigue at room temperature. Several specimens were tested at each stress level. A plot of stress versus cycles to failure is presented in Figure 3. At a stress level of 140 MPa, we can see that fatigue lives ranged from approximately 10 cycles up to 20,000 cycles. That is over three orders of magnitude in fatigue life, while in metals, the spread in fatigue lives is typically at 2×.

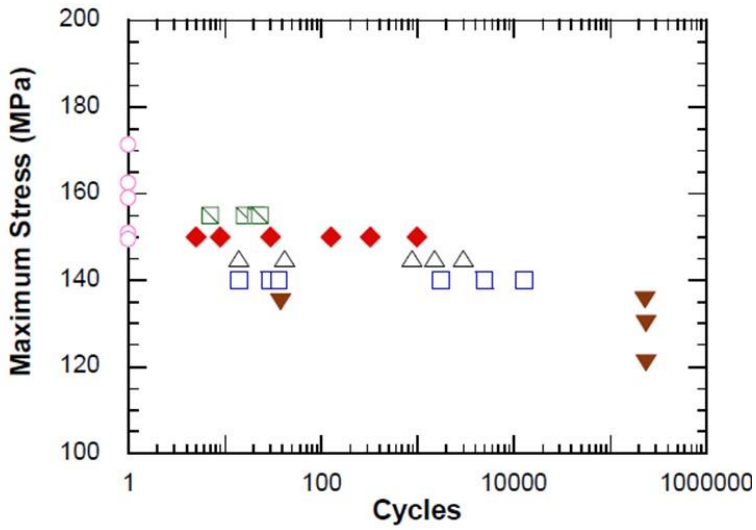

Figure 3. Stress Versus Cycles for SiC/SiC Tested at 23°C [3]

The ASTM tension test study by Gonczy did not exhibit significant variation in UTS, while the fatigue testing by Reynaud revealed a very large spread in fatigue lives. With this in mind, it was decided that it would be important to address issues associated with variability in CMCs at elevated temperature, and for a durability test such as fatigue or creep rupture. An oxide/oxide system was selected, as it would avoid the significant environmental oxidation issues associated with SiC/SiC CMCs. Stress rupture was selected because oxide/oxide CMCs exhibit limited fatigue damage, but do exhibit significant strain deformation when exposed to static loads while at temperature.

DISTRIBUTION STATEMENT A. Approved for public release: distribution is unlimited.
88ABW-2019-2847

3 MATERIALS DESCRIPTION

3.1 Description of N720/AS

The oxide/oxide CMC material system selected for this study was manufactured by COIC using a sol-gel technology. It is made using commercially available 3M[2] Nextel™720 (mullite) fibers that are commercially available from 3M and a matrix-based on alumino-silicate (AS) chemistry. For the remainder of the report, this CMC will be referred to as N720/AS.

N720/AS was selected for this variability study for several reasons. The primary reason is that it is one of the more mature CMC systems. Therefore, there would be less chance of random processing issues arising during manufacturing. The second main reason is that that sol-gel processing methodology is far less complicated than for other CMC systems, such as polymer infiltration and pyrolysis (PIP) or silicon melt infiltration of SiC/SiC. In addition, the cost of this CMC is approximately one-fourth that of advanced SiC/SiC CMCs.

3.2 Processing Of N720/AS

A schematic of the processing methodology is presented in Figure 4. A total of three plates (Numbers 1447-16, 1447-17, and 1447-20) of material were purchased for this study. They were made at the same time using the same equipment and staff. Each panel was machined by COIC into 12 test specimens. Ten specimens from each plate were tested for stress rupture life, while one was tension tested at 1100°C. The purchase order required the manufacturer to meet a certain UTS value. Therefore, the twelfth specimen from each plate was tensile tested by the material manufacture at room temperature to verify tensile strength before delivery.

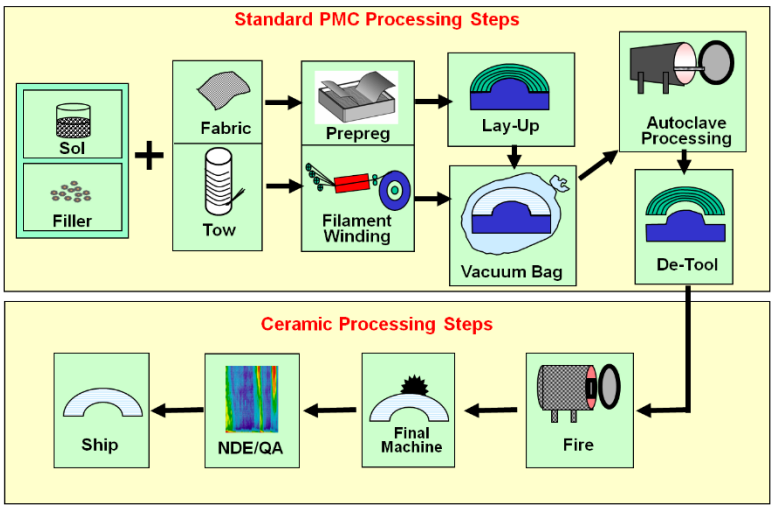

Figure 4. Schematic of Processing Methodology Used to Make N720/AS

[2] 3M Products, 3M Corporate Headquarters, 3M Center, St. Paul, MN 55144-1000.

DISTRIBUTION STATEMENT A. Approved for public release: distribution is unlimited.
88ABW-2019-2847

3.3 Microstructure Studies of N720/AS

A room-temperature-tested tensile specimen was used for the microstructural studies. The tab region of the test specimen was sectioned as shown in Figure 5. The cuts were made 90° and 45° from the long axis (loading direction) and the microstructure was documented using optical microscopy. The authors have found that sectioning at 45° allows for excellent viewing of all the fibers in the entire cross section with little to no polishing damage; whereas, 90° cuts often have many fibers pulled out during polishing. The follow micrographs were taken from Sections B and E and C.

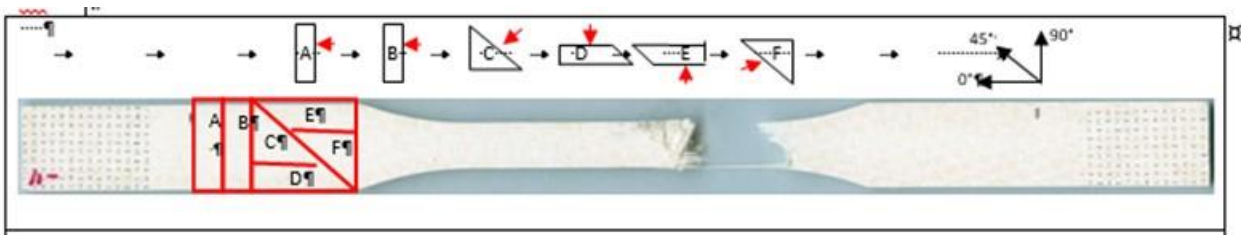

Figure 5. Photo of Tested N720/AS Specimen and Location of Cuts Made for Microstructural Studies

The entire 0/90 cross-section of the test specimen is captured in Figure 6, which is perpendicular to the loading direction (B) and Figure 7, which is parallel to the loading direction (E). In both these images, there are small pores (~200-300 microns in length), but are few in number and well spread out. The 12 plies can easily be identified. There appear to be some thin strips of matrix-rich regions between the plies, but overall, the CMC is very well densified and the microstructure is very uniform. In the figure, there is an absence of any large matrix-shrinkage cracks that are often observed in oxide/oxide CMCs. Figure 8 was taken at 200× and provides excellent documentation of the general microstructure. The individual fiber tows have been very well infiltrated, and the compaction during autoclave cure resulted in very few matrix-rich regions between the plies. There are only a few very small fiber-sized pores located within the fiber tows. Figure 9 was taken at 500× and, again, there appears to be very good infiltration of the fiber tows. At this magnification, it is now possible to identify some of the matrix shrinkage cracks that occur during processing. Even at very high magnification of 1000×, it can be observed that the fiber tows are completely infiltrated with matrix.

DISTRIBUTION STATEMENT A. Approved for public release: distribution is unlimited.
88ABW-2019-2847

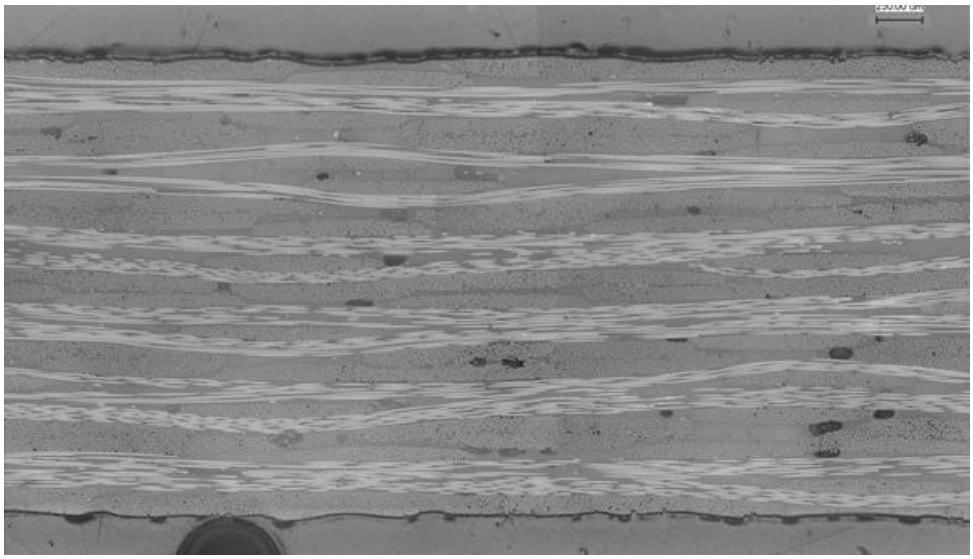

Figure 6. Low-Magnification 0/90 Micrograph of Entire Cross Section of N720/AS Test Specimen (100×, B)

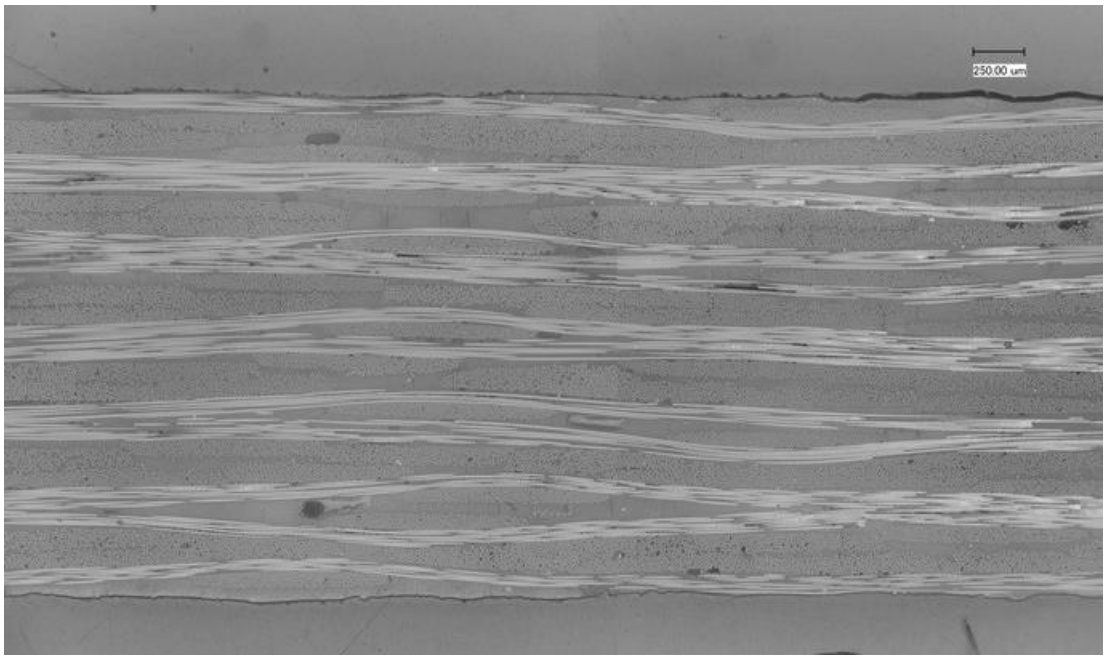

Figure 7. Low-Magnification 0/90 Micrograph of Entire Cross Section of N720/AS Test Specimen (100×, E)

DISTRIBUTION STATEMENT A. Approved for public release: distribution is unlimited.
88ABW-2019-2847

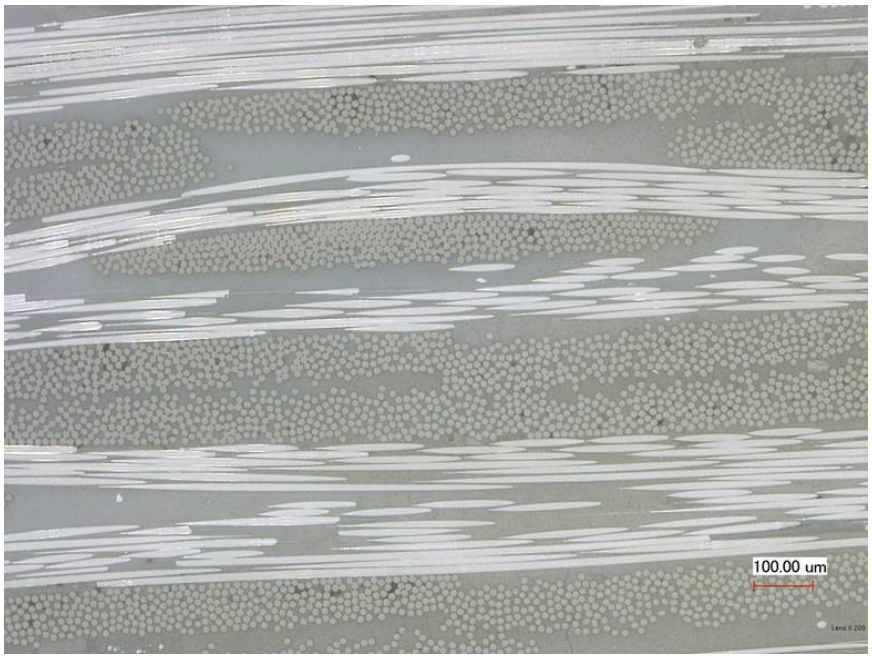

Figure 8. Representative 0/90 Micrograph of N720/AS Microstructure (200×, B)

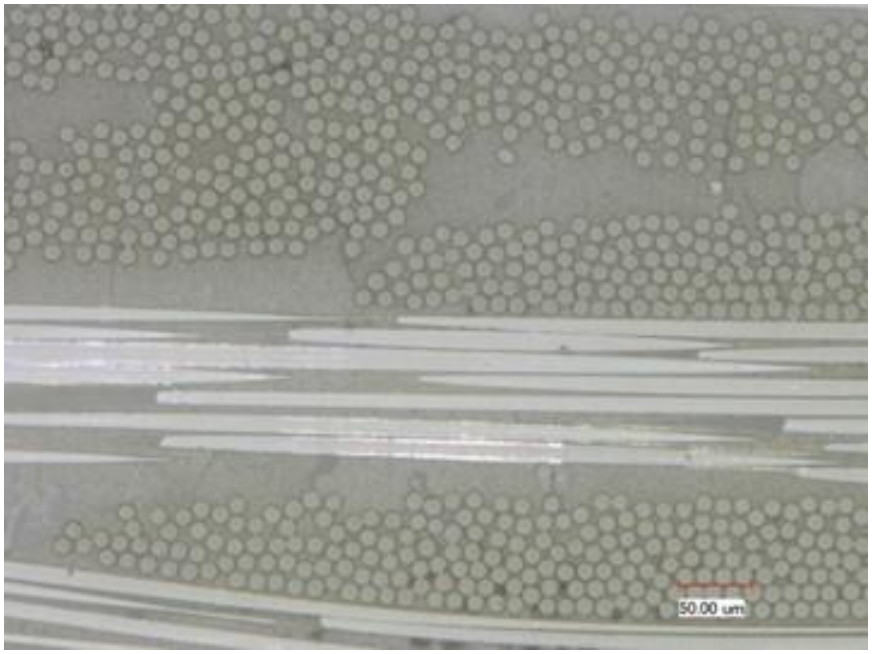

Figure 9. Representative 0/90 Micrograph of N720/AS Microstructure (500×, B)

DISTRIBUTION STATEMENT A. Approved for public release: distribution is unlimited.
88ABW-2019-2847

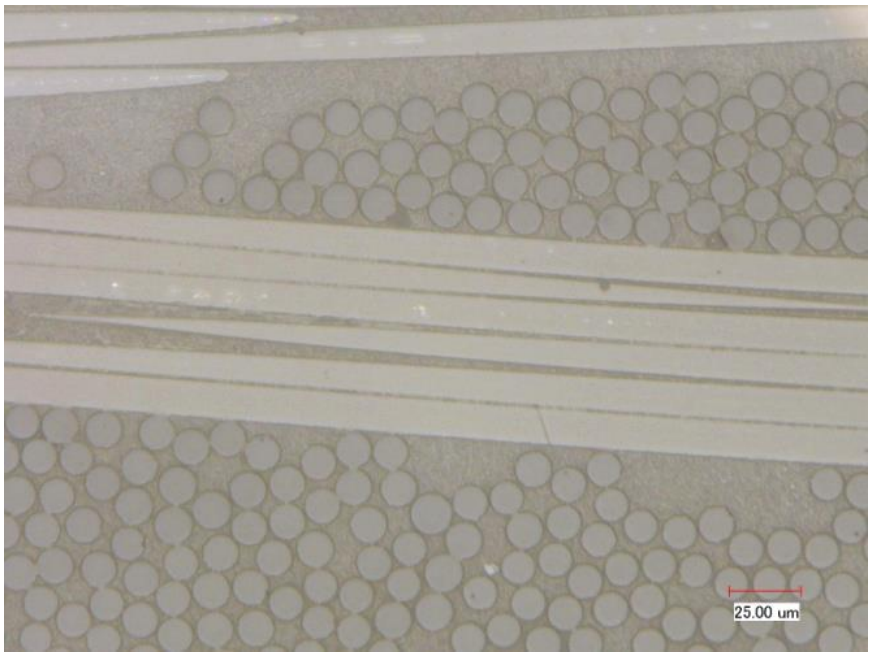

Figure 10. Representative 0/90 Micrograph of N720/AS Microstructure (1000×)

As stated earlier, there are many advantages to sectioning and polishing at 45° to the fiber directions, such as allowing for excellent viewing of all fibers in the entire cross section with little to no polishing damage. A low-magnification image of the entire cross-section of Section C is shown in Figure 11. In this image, the small 200- to 300-micron pores can still be seen and are, once again, few in number and spaced well apart. One feature that is much easier to identify is the matrix-rich regions and it can be observed that there are only very small strips between each of the plies. The composite plies appear to have nested well, and none of these matrix-rich regions extends beyond one fiber tow. An image taken at 200× is presented in Figure 12 and is a great example of the general microstructure. In this image, the fiber tow bundles appear to be completely infiltrated and the matrix-rich regions only appear as thin strips that are not longer than the individual fiber tows. At 500×, as shown in Figure 13, the matrix shrinkage cracks are, once again, visible, but are small with very limited crack mouth opening displacements. Figure 14 was taken at 1000× and, at this magnification, a few very small fiber-sized pores can be observed within the fiber tow bundles. A scanning electron microscope (SEM) was also used to image the CMC. Figure 15 is a high-resolution SEM image where one can begin to see the porous nature of the AS matrix. However, even at this very high magnification, the matrix has infiltrated around all of the fibers – even when the space between fibers is only 1 to 2 microns.

Overall, the microstructural studies of this N720/AS CMC have revealed that the composite was very well infiltrated and densified, and that there are no glaring defects in the microstructure. The fiber and fiber tow distributions appear to be very good, with the only defect being the occasional 200- to 300-micron size pore that sometimes occurs between fiber tows.

DISTRIBUTION STATEMENT A. Approved for public release: distribution is unlimited.
88ABW-2019-2847

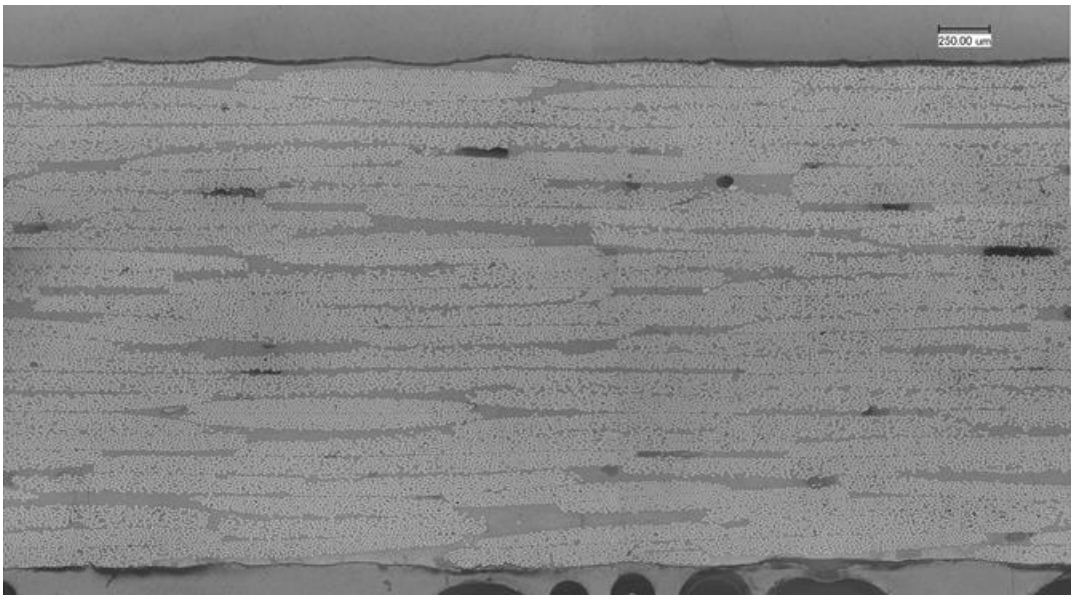

Figure 11. Representative ±45 Micrograph of N720/AS Microstructure (C)

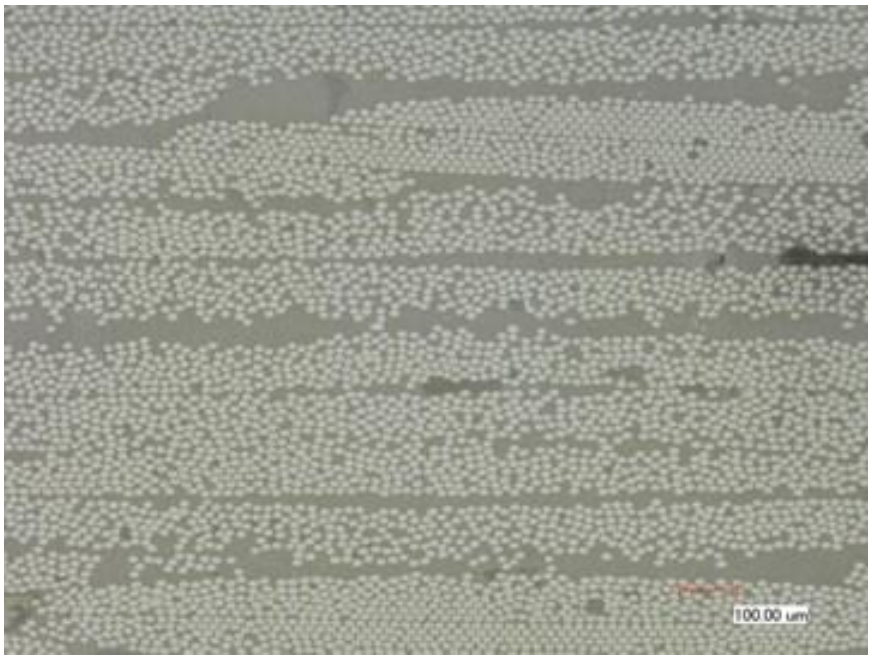

Figure 12. Representative ±45 Micrograph of N720/AS Microstructure (200×, C)

DISTRIBUTION STATEMENT A. Approved for public release: distribution is unlimited.
88ABW-2019-2847

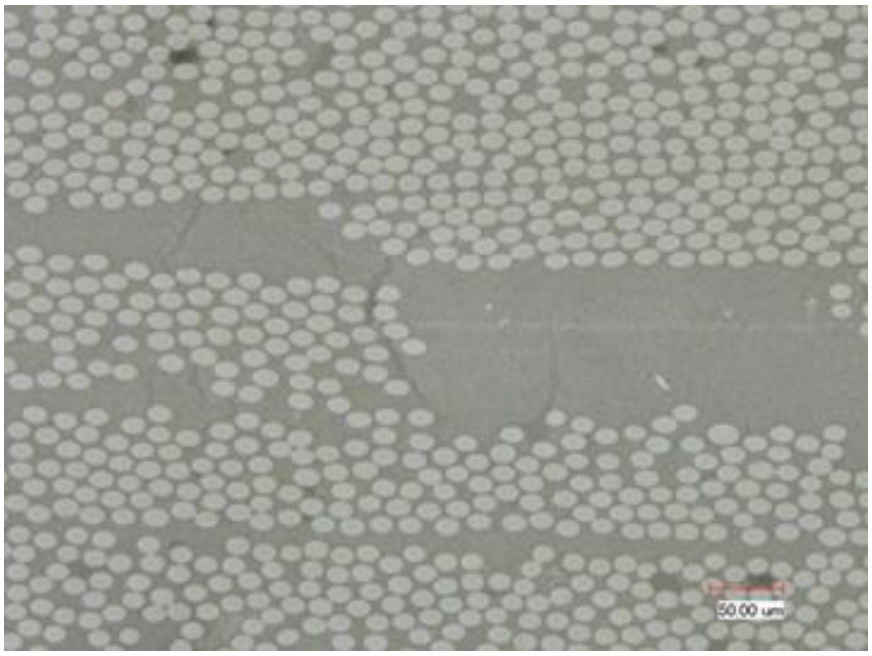

Figure 13. Representative ±45 Micrograph of N720/AS Microstructure (500×, C)

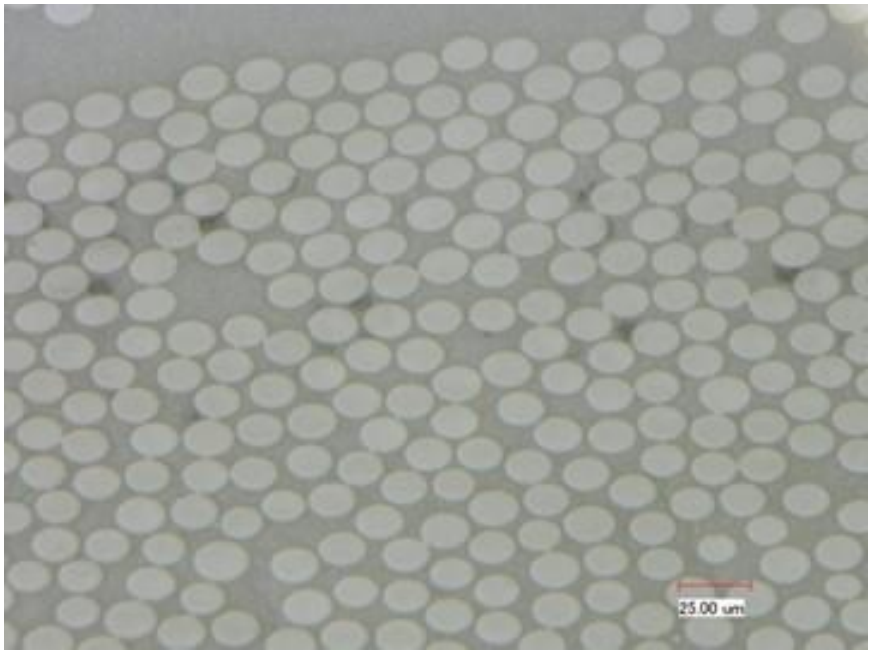

Figure 14. Representative ±45 Micrograph of N720/AS Microstructure (1000×, C)

DISTRIBUTION STATEMENT A. Approved for public release: distribution is unlimited.
88ABW-2019-2847

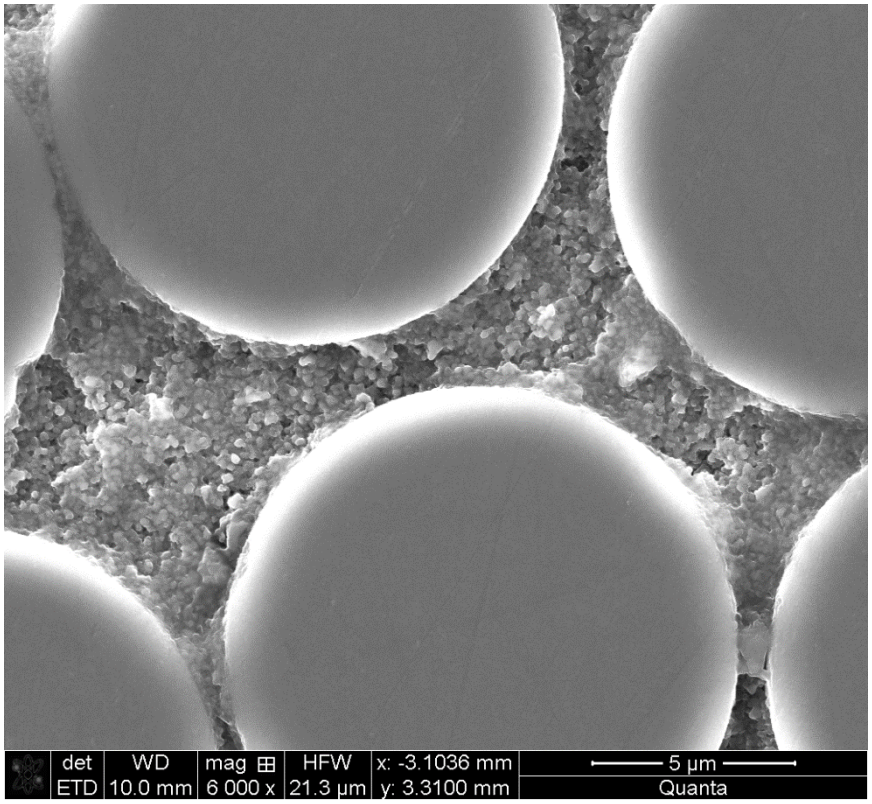

Figure 15. High-Resolution SEM Image of N720 Fibers and Porous Alumino-Silicate Matrix (6000×)

In addition to studying the general microstructure, the optical images were used to measure the fiber volume fraction for each panel. The point-count method was used and the results are presented in **Error! Reference source not found.**, along with density measurements provided by COIC. It appears that the three panels have nearly identical fiber volume fractions and densities. This is not surprising, and the excellent uniformity is the primary reason this N720/AS system was selected for this investigation.

Table 3. Fiber Volume Fractions and Density of N720/AS Panels

Plate	Vf	Density
1447-16	47.3	2.65
1447-17	47.0	2.65
1447-20	47.4	2.64

DISTRIBUTION STATEMENT A. Approved for public release: distribution is unlimited.
88ABW-2019-2847

4. TESTING PROCEDURE

All tension and stress rupture tests were axial loaded and performed on materials with a cross-ply (0/90) fiber architecture. Specimens were machined such that the outer ply warp direction was always parallel to the loading direction.

4.1 Test Specimen Geometry

A dogbone test specimen geometry (standard AFRL/RXCCP design) was used for the tension and stress rupture tests in this study. A specimen length of 175 mm was selected to allow the grips to be far enough away from the furnace body to avoid exceeding temperature recommendations of the grip manufacturer during the stress rupture testing at 1100°C. This length also allowed use of insulation between the furnace and the grips. Gauge length was selected to be 28 mm to allow for a 25.4 mm extensometer to be used to measure strain. Tab width was selected to be 15 mm and gage width 8 mm. The ratio of the gage section width to the grip tab width was selected to be 53%. This reduction has been shown to be sufficient to produce gage section failures for specimens that exhibit tensile strengths up to 500 to 600 MPa. A gage width of 8 mm was selected due to the oxide/oxide CMC system being manufacture with an eight-harness satin-weave (8HSW) fiber architecture. An 8HSW has a repeating distance of approximately 8 mm, so this allows for one complete unit cell for the 8HSW architecture. AFRL/RXCCP normally uses a radius of 50 mm to minimize the transition length of the radius from the machined gage section to the tab area in order to avoid intermediate temperature embrittlement (ITE), which is very common among many SiC fiber-based CMCs.

A linear elastic finite-element study of this radius and specific specimen dimensions revealed that it generated a small localized region at the initial transition region of the radius where the stress was 4.4% higher than in the uniform cross-section stress in the gage section. Prior testing on several types of CMCs has shown that this radius and corresponding localized stress concentration typically produced failures that are randomly located across the gage section, with failure rarely occurring at the beginning of the radius on the test specimen.

The CMC manufacturer was requested to make panels with a final thickness of ~2.5 mm, which resulted in a total of 12 plies for each CMC panel. Thickness of the test specimens was left at as-produced. It is desirable to keep specimen thickness below 3 mm, as it reduces the amount of gripping force required to pull the specimen to failure without generating griping damage and grip failures. A schematic of the test specimen design is shown in Figure 16.

DISTRIBUTION STATEMENT A. Approved for public release: distribution is unlimited.
88ABW-2019-2847

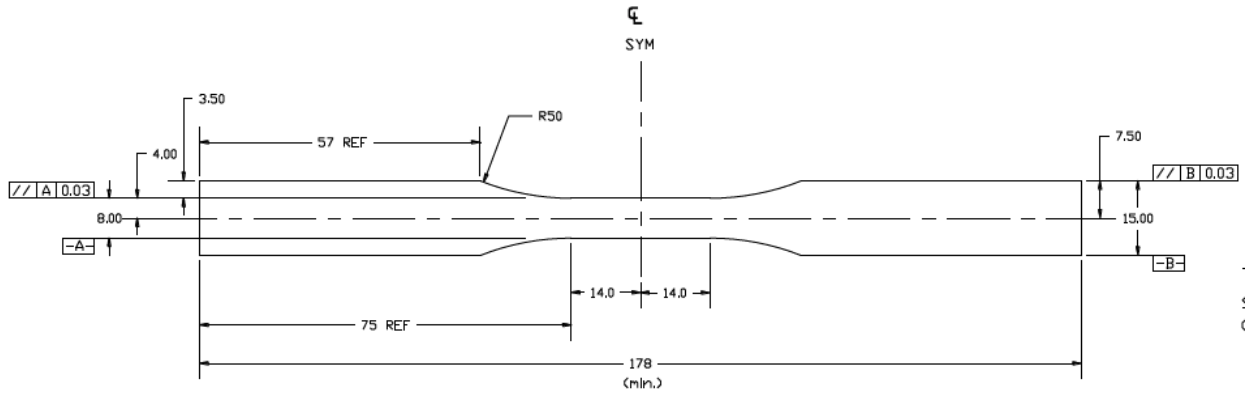

Figure 16. Schematic Diagram of Dogbone Test Specimen Geometry Used for N720/AS Stress Rupture Variability Study

4.2 Test Frame and Grips

Testing was performed using a horizontal servo-hydraulic test system (SH#12), shown in Figure 17, which was specifically designed for testing CMCs. It is uniquely orientated in the horizontal configuration and equipped with custom-designed, water-cooled, friction-clamping grips; a MTS Systems Corporation (MTS) 609 alignment device; 5.5-kip (25kN) MTS load cell; MTS 458 analog Micro-Console signal controller; and UDRI-developed MATE (material analysis and testing) test control and data acquisition software.

This test frame utilized a unique purpose-built gripping system designed to achieve a very high degree of alignment while providing a fixed-fixed clamping condition ideal for strain-limited materials. The coefficient of friction between the specimen and the specially prepared surface of the metal inserts are leveraged to optimize pressures required. These economical grips use a clamping action, driven by a pneumatic-to-hydraulic ram inside a yoke, and utilize removable metal inserts to accommodate different thickness specimens. Careful selection of the inserts results in very little movement of the grip faces, and this both reduces the chance of pinching the specimen and maintains the high degree of alignment. The grip bodies are water cooled while the metal inserts in contact with the specimen are not cooled.

The test frame was designed and built in the horizontal configuration specifically for characterization of the mechanical properties of low-strain materials at very high temperatures. Furnaces that operate in the vertical position experience significant heat rising within the furnace – commonly called the “chimney” effect. This rising heat makes it very hard to produce a uniform temperature in the gage section of the test specimen, as the lower end is almost always cooler than the top. Multiple heating zones can minimize this effect, but only to some degree. In contrast, furnaces operated in the horizontal orientation produce a very uniform and symmetric temperature profile in the gage section of the test specimen. Also, the high-temperature extensometer mounting arrangement requires substantially less force to keep it in contact with the test specimen.

DISTRIBUTION STATEMENT A. Approved for public release: distribution is unlimited.
88ABW-2019-2847

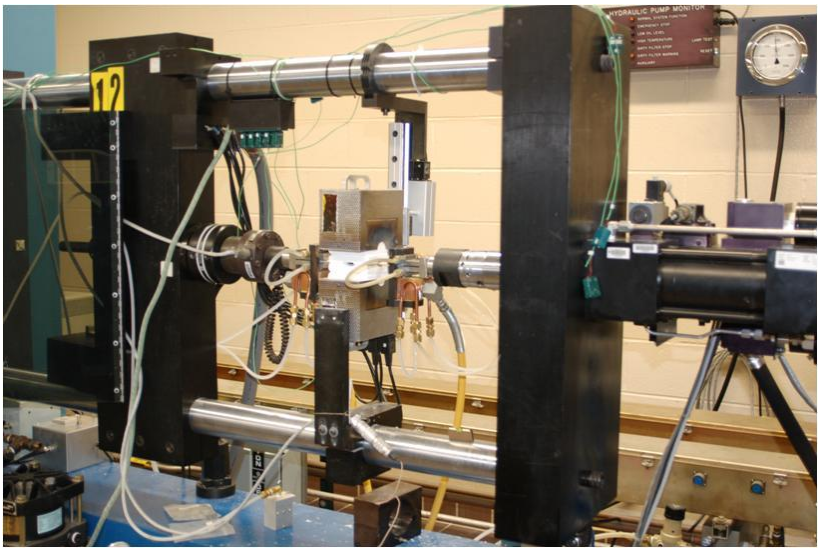

Figure 17. Photograph of Test System (SH#12) Used for Stress Rupture Testing

Testing at elevated temperatures on SH#12 is achieved using a three-zone hot-rail furnace manufactured by Amteco, Inc. and discussed in detail in Section 4.4. This furnace utilizes a commonly used split design and three SiC heating elements in each half. There are three S-type control thermocouples within the furnace cavity allowing for three zones of temperature control.

4.3 Test Frame Alignment

Alignment is very important when testing CMCs, as they typically only exhibit 0.3% to 0.5% strain to failure. To align the load train of the test machine, an MTS Model 609 alignment device was used to adjust concentricity and angularity. The grip/load train alignment was verified using a precision-ground, hardened steel, straight-sided specimen instrumented with eight strain gages, as shown in Figure 18. The machine was aligned according to ASTM E1012-14, "Standard Practice for Verification of Testing Frame and Specimen Alignment Under Tensile and Compressive Axial Force Application".[4] ASTM requirements for testing CMCs in tension or creep rupture state that there is to be less than 5% bending at 500 με average axial displacement for all four specimen alignment orientations. A plot of percent bending versus axial strain is presented in Figure 19, showing percent bending drops below 5% at only ~100 με. At 500 με, the percent bending was measured to be slightly less than 2%. Such a low value of bending indicates the test machine load train is very highly aligned and removes from the variability study any contributions from miss-alignment.

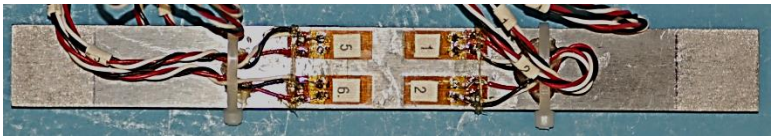

Figure 18. Straight-Sided Steel Bar Alignment Specimen with Eight Strain Gages

DISTRIBUTION STATEMENT A. Approved for public release: distribution is unlimited.
88ABW-2019-2847

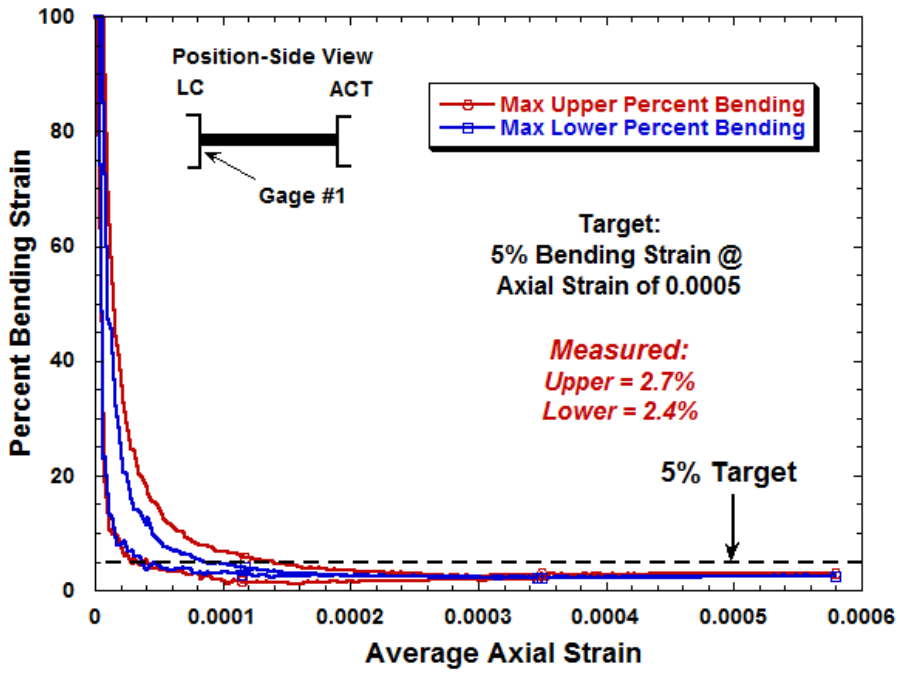

Figure 19. Plot of Percent Bending Versus Average Axial Strain

4.4 Furnace and Thermal Profiling

As stated, the elevated-temperature testing was conducted using a commercially available three-zone furnace made by Amteco, Inc. A photograph of the furnace mounted in the test frame is shown in Figure 17 and a side view in Figure 20. This split-design furnace uses three silicon-carbide heating elements in each furnace half which are similar to the ignitor elements used in house furnaces. There are three S-type control thermocouples (TC) within the furnace cavity allowing for three zones of automated temperature control. Insulation pieces with specimen and instrumentation cut-outs were placed between the two furnace halves to help both preserve the integrity of the furnace cavities and to help keep the furnace well-sealed. Having the furnace in a horizontal position allowed for the use of these easily replaced insulation cutouts. Before the test matrix was started, the three-zone igniter furnace was completely rebuilt with new insulation, heating elements, and control thermocouples. For operation, the furnace was packed with customized insulation pieces in a repeatable fashion for every test.

DISTRIBUTION STATEMENT A. Approved for public release: distribution is unlimited.
88ABW-2019-2847

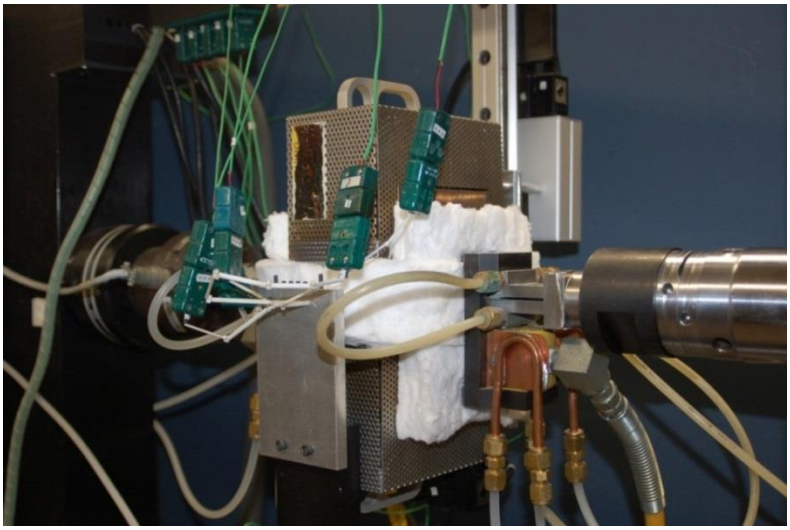

Figure 20. Side View of Amteco Furnace Showing Custom-Built Gripping System Developed for Flat CMC Specimens

A schematic of the furnace showing the three control and five thermal mapping/ profiling TCs is shown as Figure 21. Photographs of a N720/AS test specimen being instrumented for temperature profile measurements are shown in Figure 22 and Figure 23. The TCCs used for the temperature mapping were bonded directly to a N720/AS test specimen and labeled as "Specimen TC." For this study, it was decided that an extremely detailed thermal profile mapping of the test specimen was required. Therefore, a total of eleven TCs were bonded to the test specimen – five to record the gage section and the remaining six recorded the temperature beyond the gage section. The three furnace zones are controlled by TCs that enter the furnace several millimeters below the test specimen and the tips are sealed with ceramic adhesive – referred to as "Furnace TC." In addition, three TCs are inserted between the two halves of the furnace and brought very close (~3 mm) to the gage section edge of the test specimen to represent the furnace air temperature at that location. They are labeled "Witness TC", and the ends are sealed with adhesive to avoid reactions with the test specimen (Figure 24). The calibration procedure involves adjusting the temperature set-point of the Furnace TC until the Specimen TC reaches both the desired maximum temperature and temperature profile along the length – the Witness TCs only being used for additional reference. For each thermal profile run, adjustments were made until the temperatures along the entire 28 mm of the machined gage length of the test specimen were within ±1% of the target test temperature, which for this study, was 1100°C. Once all TCs were in place, the top furnace half was lowered into place and additional insulation added between the furnace and grips, as shown in Figure 25.

An example temperature calibration run for a N720/AS test specimen is presented in **Error! Reference source not found.**. The table lists the actual Specimen TC temperatures measured for the final calibration run at 1100°C (also presented graphically in Figure 26), along with values for the Furnace TC and Witness TC. The data clearly documents that the Specimen TCs are all within +0.1/- 0.7% of 1100°C. Great care was taken to achieve this excellent thermal profile in order to remove that as a potential contributing source of variability for the stress rupture tests.

DISTRIBUTION STATEMENT A. Approved for public release: distribution is unlimited.
88ABW-2019-2847

Witness TC temperatures are10°C to 20°C below those measured on the test specimen, even though they are essentially right next to the edge of the test specimen. The Furnace TCs are significantly lower, at 25°C to 33°C below those measured on the test specimen. The data clearly demonstrate why one cannot simply use the Probe TC located inside this type of furnace to conduct high-temperature testing on advanced CMCs and C/Cs. Documentation of the Furnace TC set points allowed for automatic control of the furnace temperature without having to bond thermocouples to the test specimens, eliminating any chance of having an adverse reaction between the TC or bonding material and the test specimen at these elevated temperatures. A detailed description of the furnace, operating procedure, and temperature profiles is proved in a separate report [5].

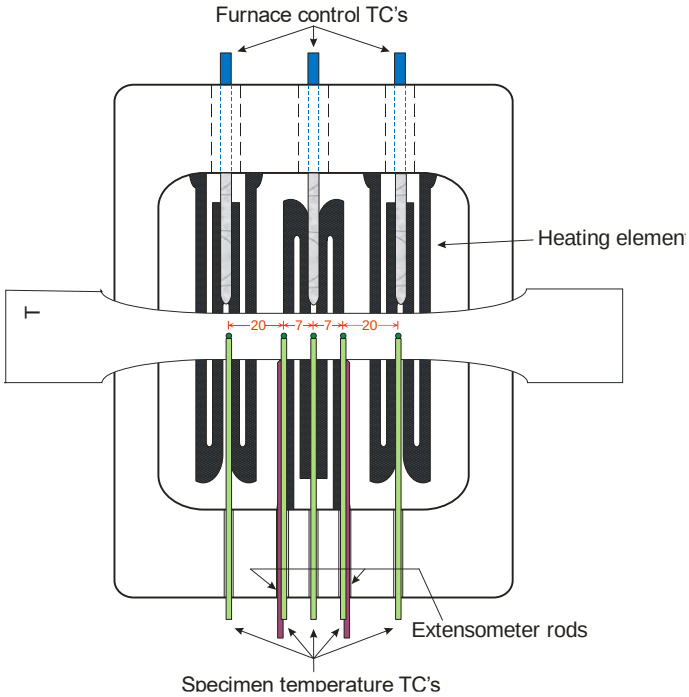

Figure 21. Schematic Showing Placement of Thermocouples for Thermal Profiling

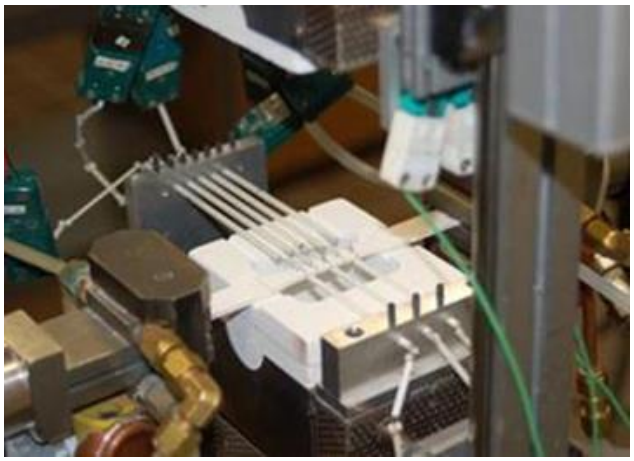

Figure 22. Furnace Setup for Thermal Profile of N720/AS Test Specimen Using 11 Thermocouples

DISTRIBUTION STATEMENT A. Approved for public release: distribution is unlimited.
88ABW-2019-2847

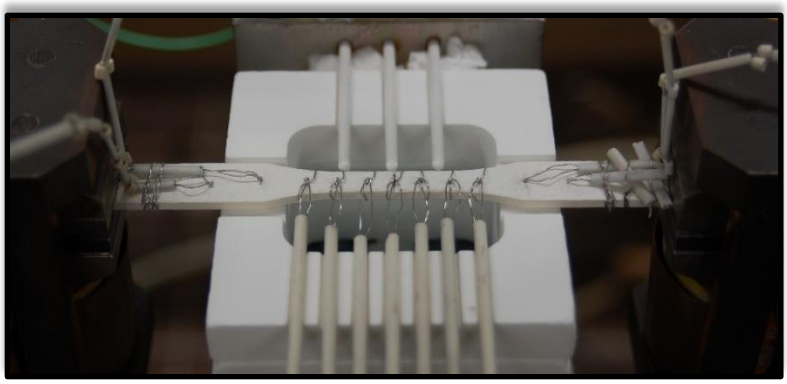

Figure 23. Photograph of N720/AS Test Specimen Instrumented with Thermocouples for Temperature Profiling

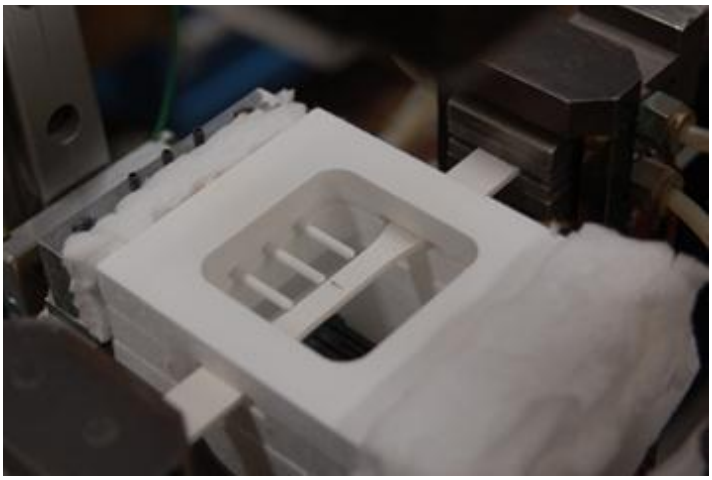

Figure 24. Photograph of Test Setup Showing N720/AS Test Specimen with Three Probe Thermocouples in Place

Figure 25. Photograph of Furnace Packed with Custom-Cut Insulation

DISTRIBUTION STATEMENT A. Approved for public release: distribution is unlimited.
88ABW-2019-2847

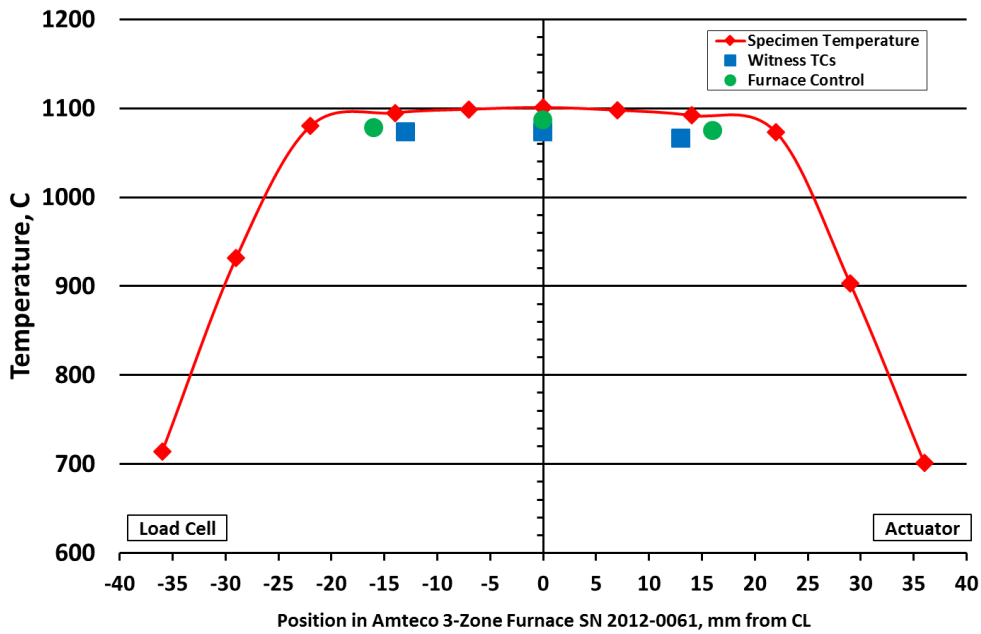

Figure 26. Thermal Profile of N720/AS Test Specimen at 1100°C

Table 4. Temperature Measurements from All Thermocouples Used for 1100°C Thermal Profile of N720/AS Test Specimen

Specimen Thermocouples			Whitness Thermocouples			Furnace Thermocouples	
(mm)	(C)		(mm)	(C)		(mm)	(C)
-36	714		-13	1074		-16	1080
-29	932		0	1074		0	1091
-22	1080		13	1067		16	1080
-14	1095						
-7	1099						
0	1101						
7	1098						
14	1092						
22	1073						
29	903						
36	701						

Note: Measurements are from Center line of Test Specimen,
Note: Negative value towards Load Cell. Positive Distance is towards Actuator

4.5 Testing Procedure for Tension Testing

All tension tests were performed on SH#12 in accordance to ASTM C1275-00, "Standard Test Method for Monotonic Tensile Behavior of Continuous Fiber-Reinforced Advanced Ceramics with Solid Rectangular Cross-Section Test Specimens at Ambient Temperatures" [6] and ASTM 1359-96, "Standard Test Method for Monotonic Tensile Behavior of Continuous Fiber-Reinforced Advanced Ceramics with Solid Rectangular Cross-Section Test Specimens at Elevated Temperatures" [7]. Displacement was measured with a high-temperature alumina rod capacitance-type extensometer for elevated tests. Each specimen was carefully aligned in the

DISTRIBUTION STATEMENT A. Approved for public release: distribution is unlimited.
88ABW-2019-2847

test machine grips and a minimum of three modulus checks performed using a maximum load of 25 MPa. Test procedure required that each of these three modulus measurements be within ±10% of the average before a tension test could be conducted. Modulus checks were performed both at room temperature and at the test temperature. During tension testing, the specimen was loaded at a rate of 10 MPa/s to failure. Load and displacement were recorded at a rate of 10 data points per second. After failure, the specimen was allowed to cool to room temperature, removed from the test frame, and the failure location measured from the end of the specimen located at the load cell side of the load train. After each test value for E, PL, UTS, and ε_f were determined and recorded.

4.6 Test Procedure for Stress Rupture Testing

Stress Rupture testing was performed in accordance with ASTM C-1337, "Standard Test Method for Creep and Creep Rupture of Continuous Fiber-Reinforced Ceramic Composites under Tensile Loading at Elevated Temperatures" [8]. For this study, the following definitions are used. Creep is described as the time-dependent strain that occurs after the application of a load, which is thereafter maintained constant. Creep rupture is a test in which both progressive specimen deformation (strain accumulation) and the time to rupture are measured. Stress rupture testing is a test in which time to rupture is measured, but no deformation measurements are made.

A total of 30 stress rupture tests s were conducted at 1100°C at a maximum stress of 175 MPa. The furnace was ramped to temperature in approximately 30 minutes and then allowed to equilibrate for 15 minutes. Load was then ramped at 10 MPa/s up to 175 MPa and held constant. For all tests, the data collected included stress, stroke, time, as well as the laboratory temperature and humidity.

The ASTM tension test round-robin by Gonczy utilized three panels and ten specimens per laboratory, and the test results from each laboratory were easily analyzed. These results produced excellent findings. Therefore, it was decided to also test three panels of ten specimens each, for a total of 30 specimens. It is always a tradeoff between number of repeat tests and cost, but it was felt that this should be a sufficient amount of test data to allow for empirical documentation of factors that influence stress rupture life.

DISTRIBUTION STATEMENT A. Approved for public release: distribution is unlimited.
88ABW-2019-2847

5. TEST RESULTS

The following sections discuss the tensile and stress rupture behavior of N720/AS.

5.1 Tensile Results

In an earlier investigation, several room-temperature tension tests were performed and are presented in **Error! Reference source not found.**. Test results for this investigation at 1100°C are presented in **Error! Reference source not found.** for Panels 1447-16, 1447-17, and 1447-20 from this investigation as well as test data from an earlier investigation. The room-temperature UTS was measured to be 229 MPa, while the strength at 1100°C was found to increase to 245 MPa. It is not uncommon to see the UTS increase between room temperature and elevated temperature for CMCs. This increase is often attributed to residual stress effects caused by thermal expansion differences between the fibers and matrix as the CMC material is cooled from its processing temperature down to room temperature. Strain to failure and the PL also increased, while the stiffness decreased only slightly. The mean UTS was measured to be 14 MPa, which is only 5.7% of the UTS, indicating good reproducibility in tensile behavior at 1100°C. The stress versus strain behavior is presented in Figure 27. All five traces lie on top of one another, documenting the repeatability of the stress-versus-strain behavior. Such tight tensile data indicates that the tensile behavior was nearly identical for the three panels, and that scatter in the data is less than that reported for S200 by Gonczy.

Table 5. Tabulated Tensile Results for N720/AS Tested at Room Temperature

Specimen ID	Panel ID	Orientation	Test Temp (°C)	Modulus Range	Modulus (GPa)	σ_{UTS} (MPa)	ε_f (%)	σ_{PL} (MPa)
11-701	1447-14	[0/90]	23	(5MPa-25MPa)	83.0	236.4	0.390	166**
11-709	1447-14	[0/90]	23	(5MPa-25MPa)	83.0	235.0	0.352	56.0
11-728	1447-15	[0/90]	23	(5MPa-25MPa)	83.7	240.1	0.379	52.4
11-795	1447-21	[0/90]	23	(5MPa-25MPa)	66.8	205.0	0.417	52.7
11-806	1447-22	[0/90]	23	(5MPa-25MPa)	77.0	227.0	0.452	55.0
				Average:	78.7	228.7	0.398	54.0
				Standard Deviation:	7.18	14.08	0.0383	1.76

Table 6. Tabulated Tensile Results for N720/AS Tested at 1100°C

Specimen ID	Panel ID	Orientation	Test Temp (°C)	Modulus Range	Modulus (GPa)	σ_{UTS} (MPa)	ε_f (%)	σ_{PL} (MPa)
11-703	1447-14	[0/90]	1100	(5MPa-25MPa)	78.2	230.0	0.409	N/A***
11-726	1447-15	[0/90]	1100	(5MPa-25MPa)	72.1	229.0	0.409	70.6
11-801	1447-21	[0/90]	1100	(5MPa-25MPa)	71.4	252.9	0.475	74.2
11-742	1447-16	[0/90]	1100	(5MPa-25MPa)	73.2	251.0	0.447	79.4
11-752	1447-17	[0/90]	1100	(5MPa-25MPa)	76.7	264.3	0.462	73.4
11-785	1447-20	[0/90]	1100	(5MPa-25MPa)	73.9	241.5	0.430	71.1
				Average:	74.3	244.8	0.439	73.7
				Standard Deviation:	2.67	13.88	0.0274	3.51

DISTRIBUTION STATEMENT A. Approved for public release: distribution is unlimited.
88ABW-2019-2847

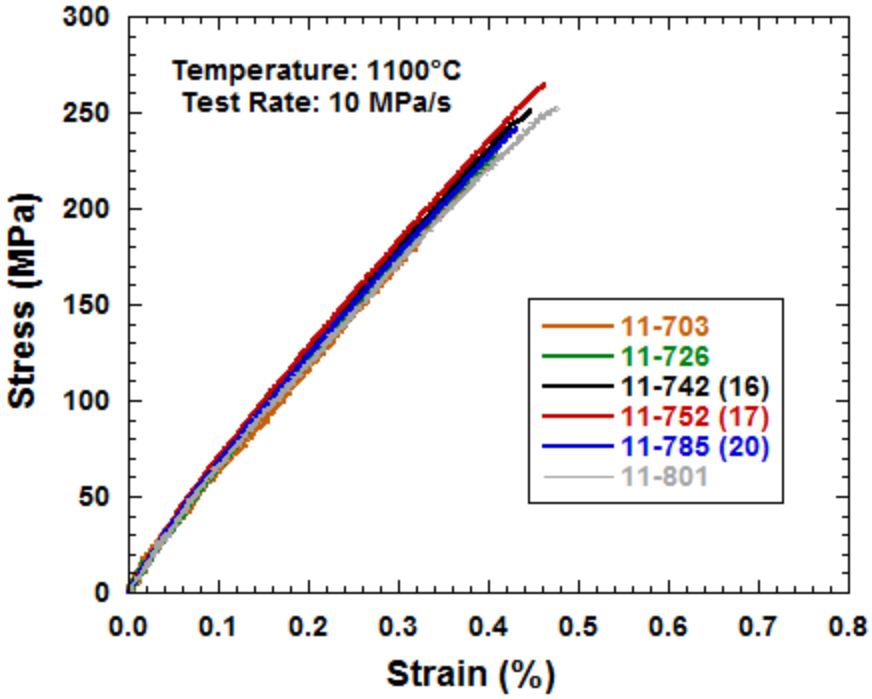

Figure 27. Tensile Stress-Versus-Strain Behavior for N720/AS at 1100°C

5.2 Stress Rupture Results

A complete listing of all recorded parameters that go into a stress rupture test, along with rupture lives, are presented in **Error! Reference source not found.** for each specimen. Also included in the table are the average values, standard deviations, and coefficient of variation. Data from several of the columns (such as time to failure, thickness measurements, and failure locations), will be addressed in detail in the Section 6 (Discussion). Overall, the average stress rupture life was determined to be 59.85 hours with a standard deviation of 26.07 hours. This is a relatively small standard deviation for stress rupture lives and indicates that the N720/AS material was very uniform.

DISTRIBUTION STATEMENT A. Approved for public release: distribution is unlimited.
88ABW-2019-2847

Table 7. Stress Rupture Testing Results of N720/AS at 1100°C

Air Force Specimen ID	Plate & Specimen ID	Average Width (mm)	Average Thickness (mm)	Average Area (mm^2)	Test Load (kN)	Target Stress (MPa)	Failure Time (h)	Failure Time (s)
11-736	1447-16-A-2	8.008	2.636	21.1087	3.6940	175	120.20	432,720
11-737	1447-16-A-3	7.954	2.706	21.5281	3.7674	175	95.54	343,944
11-738	1447-16-A-4	7.982	2.687	21.4450	3.7529	175	111.20	400,320
11-739	1447-16-A-5	7.923	2.66	21.0759	3.6883	175	109.70	394,920
11-740	1447-16-A-6	7.955	2.607	20.7394	3.6294	175	97.89	352,404
11-741	1447-16-A-7	7.994	2.682	21.4426	3.7525	175	90.78	326,808
11-743	1447-16-A-9	7.983	2.697	21.5328	3.7682	175	53.25	191,700
11-744	1447-16-A-10	7.992	2.702	21.5990	3.7798	175	57.63	207,468
11-745	1447-16-A-11	7.997	2.711	21.6825	3.7944	175	37.13	133,668
11-746	1447-16-A-12	8.012	2.699	21.6244	3.7843	175	58.48	210,528
11-747	1447-17-A-2	8.014	2.692	21.5729	3.7753	175	59.69	214,884
11-748	1447-17-A-3	8.023	2.702	21.6801	3.7940	175	83.43	300,348
11-749	1447-17-A-4	8.012	2.709	21.7080	3.7989	175	41.15	148,140
11-750	1447-17-A-5	8.036	2.733	21.9655	3.8440	175	62.65	225,540
11-751	1447-17-A-6	8.009	2.747	22.0034	3.8506	175	46.72	168,192
11-753	1447-17-A-8	8.027	2.663	21.3782	3.7412	175	70.52	253,872
11-754	1447-17-A-9	8.025	2.697	21.6480	3.7884	175	29.24	105,264
11-755	1447-17-A-10	8.048	2.713	21.8354	3.8212	175	42.57	153,252
11-756	1447-17-A-11	8.025	2.745	22.0328	3.8557	175	40.82	146,952
11-757	1447-17-A-12	8.016	2.721	21.8100	3.8168	175	41.33	148,788
11-780	1447-20-A-2	8.001	2.656	21.2499	3.7187	175	41.95	151,020
11-781	1447-20-A-3	8.005	2.692	21.5510	3.7714	175	58.01	208,836
11-782	1447-20-A-4	7.989	2.695	21.5307	3.7679	175	39.48	142,128
11-783	1447-20-A-5	8.015	2.711	21.7306	3.8029	175	50.25	180,900
11-784	1447-20-A-6	7.989	2.701	21.5783	3.7762	175	38.23	137,628
11-786	1447-20-A-8	8.015	2.717	21.7779	3.8111	175	---	---
11-787	1447-20-A-9	8.018	2.692	21.5844	3.7773	175	27.75	99,900
11-788	1447-20-A-10	7.998	2.701	21.6026	3.7805	175	30.37	109,332
11-789	1447-20-A-11	8.030	2.665	21.3977	3.7446	175	40.93	147,348
11-790	1447-20-A-12	8.016	2.608	20.9042	3.6582	175	58.90	212,040
Average		8.004	2.692	21.544	3.770	N/A	59.85	215477
Starndard Deviation		0.026	0.033	0.294	0.051	N/A	26.07	93841
Coeficient of Variation (%)		0.319	1.22	1.36	1.36	N/A	43.55	43.55

DISTRIBUTION STATEMENT A. Approved for public release: distribution is unlimited.
88ABW-2019-2847

6. DISCUSSION

6.1 Stress Versus Time to Failure

All stress-versus-linear time to failure data is presented in Figure 28, ranging from a low of 27.8 hours to a high of 120.2 hours. This same data is presented as stress versus log time to failure in Figure 29, where the lack of variability is clearly evident. The data extends over less than one order of magnitude. Figure 30 presents the same data as stress versus log time to failure in seconds. It is encouraging to see such tight data. In contrast, Reynaud observed approximately three orders in magnitude variability for room-temperature fatigue testing of a SiC/SiC composite.

Even though the total data set appears very consistent, it was important to also study the data sets from each panel. Therefore, a plot of stress versus time to failure, with each panel represented by a different symbol, is presented in Figure 31. In studying the data, it appears that Panel 1447-16 had a disproportionate amount of long-life tests. The same data is presented again in Figure 32 with separate results for each panel, along with the tensile test data UTS for each panel. In general, Panel 1447-20 exhibited the shortest lives, while Panel 1447-16 exhibited the longest. There appears to be no relationship between stress rupture lives and the measured tensile strength. To study this a bit further, a histogram plot was generated showing number of failures versus strength. This is shown as Figure 33 and it appears to show that the stress rupture times to failure have a bi-modal distribution. This is an important observation, as it indicates more than one primary damage mechanism was involved with the failure process (discussed in more detail in the following sections).

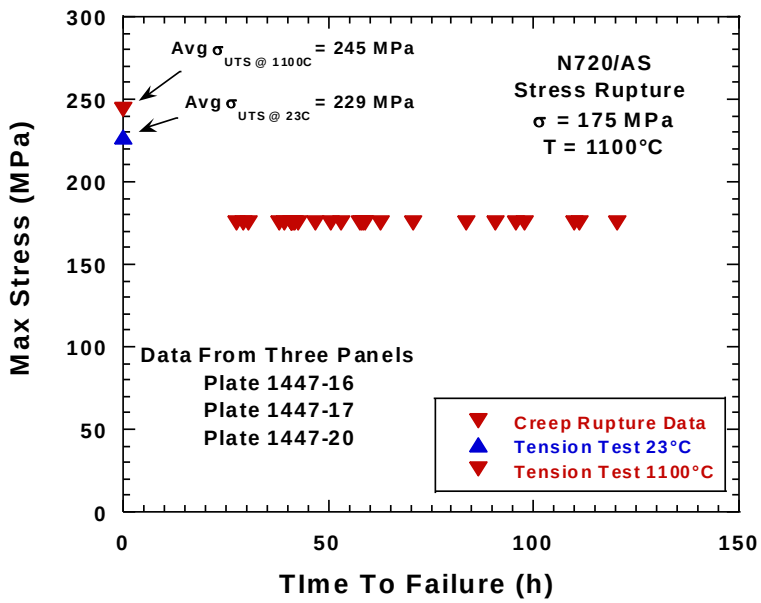

Figure 28. Stress Versus Linear Time to Failure for N720/AS

DISTRIBUTION STATEMENT A. Approved for public release: distribution is unlimited.
88ABW-2019-2847

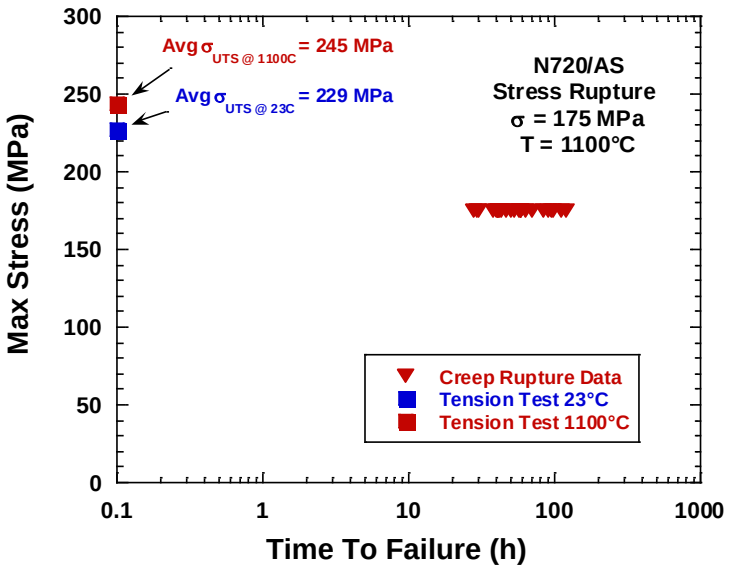

Figure 29. Stress Versus Log Time to Failure (Hours) for N720/AS

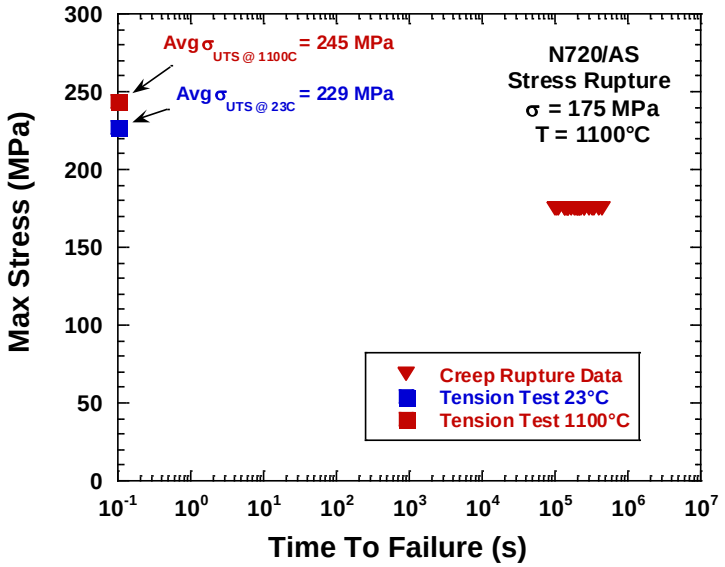

Figure 30. Stress Versus Log Time to Failure (Seconds) for N720/AS

DISTRIBUTION STATEMENT A. Approved for public release: distribution is unlimited.
88ABW-2019-2847

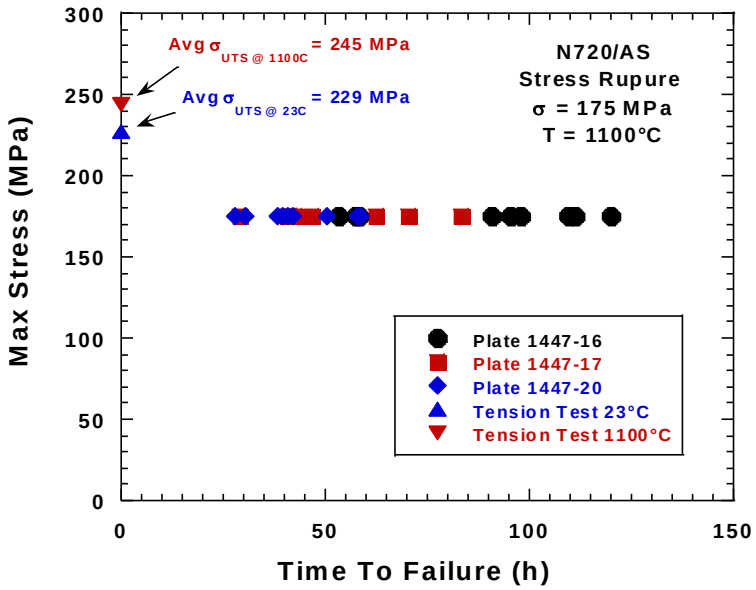

Figure 31. Stress Versus Time to Failure for Three Panels of N720/AS

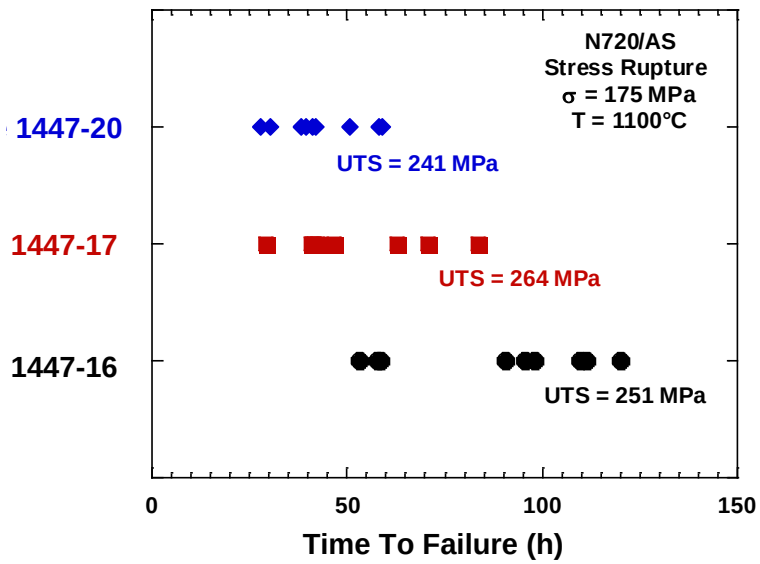

Figure 32. Stress Versus Time to Failure for Individual Panels of N720/AS

DISTRIBUTION STATEMENT A. Approved for public release: distribution is unlimited.
88ABW-2019-2847

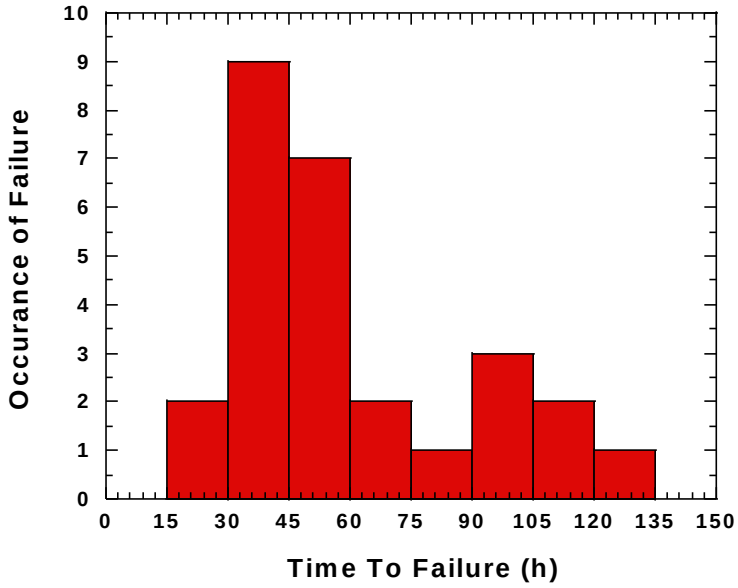

Figure 33. Histogram Plot of Time to Failure for N720/AS Showing Bi-Modal Distribution

6.2 Probability of Failure

A very useful technique for studying stress rupture lives involves probability of failure (POF), which is the likelihood that a specimen will fail at a given time and is an important part of conducting a risk analysis. A POF plot for all of the test data is presented in Figure 34. It is interesting to note that the data appears to be bi-modal in nature, with two distinct linear regions. From the stress-versus-time data presented in Figure 32, it was observed that each individual panel had a different distribution of failures. Therefore, POF was calculated for each individual panel and the results are presented in a POF plot as Figure 35. It appears that Panels 1447-17 and 1447-20 are very similar; however, Panel 1447-16 appears to have shifted to significantly longer lives for the same probabilities, and there are two distinct groupings of the test data. This suggests that Panel 1447-16 is somehow different from the other two panels as it exhibited improved stress rupture behavior, and that more than one mechanism contributed to the failure of these test specimens. The histogram plot shown in Figure 33 also suggests there were two distinct damage mechanisms operating. The following sections will attempt to address this observation.

DISTRIBUTION STATEMENT A. Approved for public release: distribution is unlimited.
88ABW-2019-2847

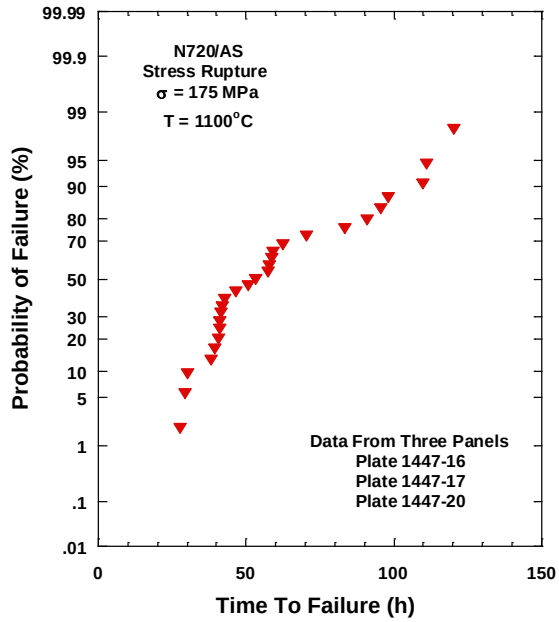

Figure 34. Probability of Failure Versus Time to Failure for N720/AS

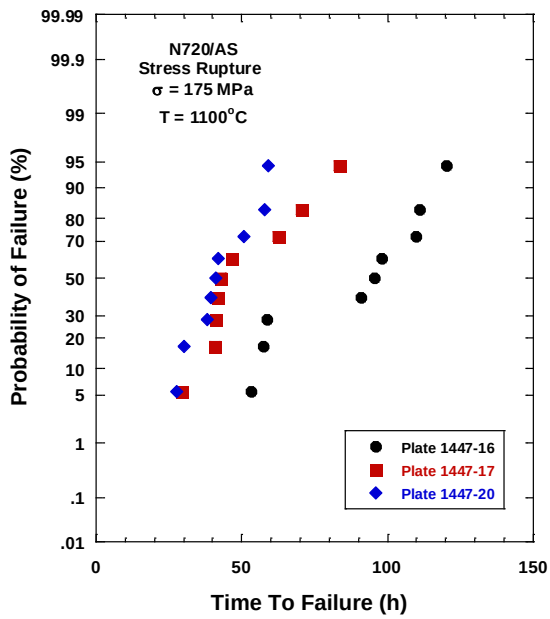

Figure 35. Probability of Failure Versus Time to Failure for Three Individual Panels of N720/AS

6.3 Humidity Effects

N720/AS was selected for this investigation primarily because it was assumed that it would not exhibit the environmental effects so often observed in SiC/SiC composites. However, as an extra precaution, the relative humidity (RH) of the laboratory was recorded throughout each stress rupture test and the tabulated results are presented in **Error! Reference source not found.** for each specimen. Figure 36 presents RH versus time for two tests. It was observed that RH often

DISTRIBUTION STATEMENT A. Approved for public release: distribution is unlimited.
88ABW-2019-2847

varied a significant amount over the length of a stress rupture test. Even so, an average RH value was calculated for each

DISTRIBUTION STATEMENT A. Approved for public release: distribution is unlimited.
88ABW-2019-2847

test specimen. A plot of RH-versus-time to failure plot is presented in Figure 37, denoting each panel with a different symbol. There is a definite trend in the data, with high average RH having the shortest lives and the lowest average RH having the longest lives. This RH data suggests that the longer lives observed for Panel 1447-16 might be attributed to the low average RH and not something inherent to the test panel itself.

Table 8. Test Specimen and Relative Humidity for N720AS Stress Rupture Tests

Specimen ID	Plate & Specimen ID	Failure Time (h)	Maximum RH (%)	Minimum RH (%)	Δ RH (%)	Average RH (%)	RH @start (%)	RH Avg First 15 min (%)	RH Avg Last 15 min (%)
11-736	1447-16-A-2	120.20	29.18	10.54	18.64	17.22	12.42	12.46	29.09
11-737	1447-16-A-3	95.54	38.50	15.54	22.96	25.90	28.99	29.16	23.92
11-738	1447-16-A-4	111.20	39.08	15.64	23.44	25.75	15.64	15.78	21.38
11-739	1447-16-A-5	109.70	38.52	11.65	26.87	20.98	13.43	13.24	24.52
11-740	1447-16-A-6	97.89	48.48	20.96	27.52	34.90	24.09	24.26	46.33
11-741	1447-16-A-7	90.78	45.32	26.18	19.14	32.54	44.61	45.08	32.33
11-743	1447-16-A-9	53.25	41.77	39.16	2.61	40.45	40.67	41.00	40.67
11-744	1447-16-A-10	57.63	48.63	36.15	12.48	40.72	44.28	44.22	47.22
11-745	1447-16-A-11	37.13	43.88	37.94	5.94	40.46	42.79	43.31	39.50
11-746	1447-16-A-12	58.48	46.89	41.67	5.22	44.15	44.64	45.66	45.25
11-747	1447-17-A-2	59.69	46.20	25.26	20.94	34.04	26.16	26.34	35.04
11-748	1447-17-A-3	83.43	46.44	17.36	29.08	25.89	17.37	17.37	46.39
11-749	1447-17-A-4	41.15	47.42	25.01	22.41	28.10	47.20	47.22	26.71
11-750	1447-17-A-5	62.65	42.78	18.95	23.83	31.69	21.31	24.26	30.90
11-751	1447-17-A-6	46.72	49.12	40.87	8.25	45.96	40.87	41.30	45.44
11-753	1447-17-A-8	70.52	51.06	44.97	6.09	47.28	49.51	49.91	46.29
11-754	1447-17-A-9	29.24	49.38	46.86	2.52	48.12	47.83	47.95	48.31
11-755	1447-17-A-10	42.57	49.95	44.71	5.24	48.23	48.98	49.35	49.06
11-756	1447-17-A-11	40.82	46.73	41.69	5.04	44.44	44.21	44.69	41.92
11-757	1447-17-A-12	41.33	43.19	39.72	3.47	41.61	40.86	41.40	42.23
11-780	1447-20-A-2	41.95	48.21	31.15	17.06	38.84	31.65	31.65	47.00
11-781	1447-20-A-3	58.01	55.99	42.34	13.65	49.78	54.48	54.55	52.44
11-782	1447-20-A-4	39.48	50.73	38.02	12.71	44.38	48.31	48.85	40.48
11-783	1447-20-A-5	50.25	42.34	31.49	10.85	37.47	40.65	40.88	32.37
11-784	1447-20-A-6	38.23	49.77	41.86	7.91	46.92	41.36	42.37	48.06
11-786	1447-20-A-8	---	---	---	---	---	---	---	---
11-787	1447-20-A-9	27.75	41.81	39.13	2.68	40.59	40.97	41.47	40.72
11-788	1447-20-A-10	30.37	63.65	41.75	21.90	50.90	49.22	49.69	42.86
11-789	1447-20-A-11	40.93	---	---	---	---	---	---	---
11-790	1447-20-A-12	58.90	49.94	38.77	11.17	46.41	38.77	39.30	44.61

DISTRIBUTION STATEMENT A. Approved for public release: distribution is unlimited.
88ABW-2019-2847

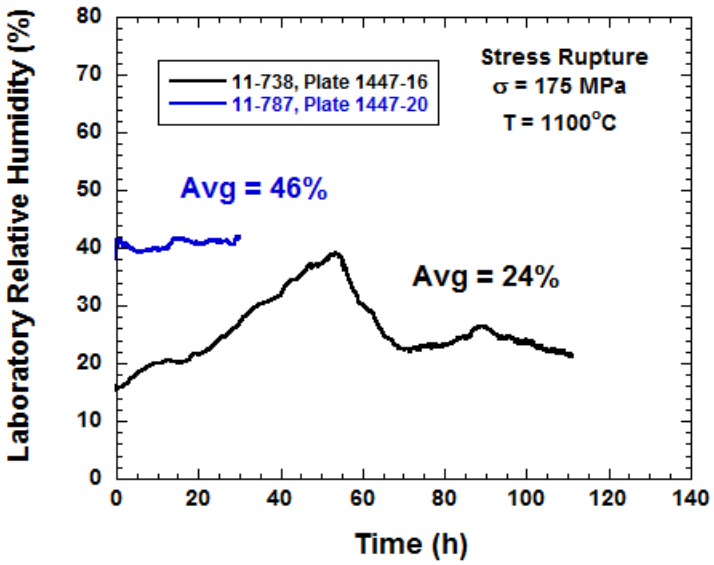

Figure 36. Plot of Laboratory Relative Humidity Versus Time

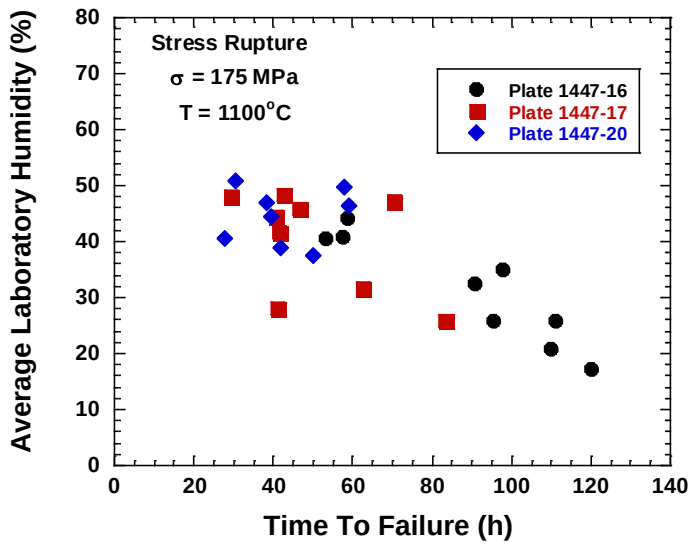

Figure 37. Average Laboratory Humidity Versus Time to Failure for N720/AS Stress Rupture Tested at 175 MPa and 1100°C

In an attempt to further study the effect of RH, the data from Figure 37 was replotted using a log scale, as shown in Figure 38. In the figure, two distinct groups of data can be observed: There is one group of test data between 35% and 55% RH and another between 15% and 35% RH. These two groupings essentially divide the RH range into two data sets that can then be used to generate a POF plot, as presented in Figure 39. The data for the range of 15% to 35% RH have approximately twice the life for each POF value as the range of 35% to 55%. The same data is plotted in Figure 40, along with the POF trace for all of the data combined. The data suggests that it is the humidity that results in the two different slopes for the combined data. Oxide/oxide CMCs are thought to be very environmentally resistant, but the stress rupture behavior observed in this study appears to be affected by humidity when tested at 1100°C.

DISTRIBUTION STATEMENT A. Approved for public release: distribution is unlimited.
88ABW-2019-2847

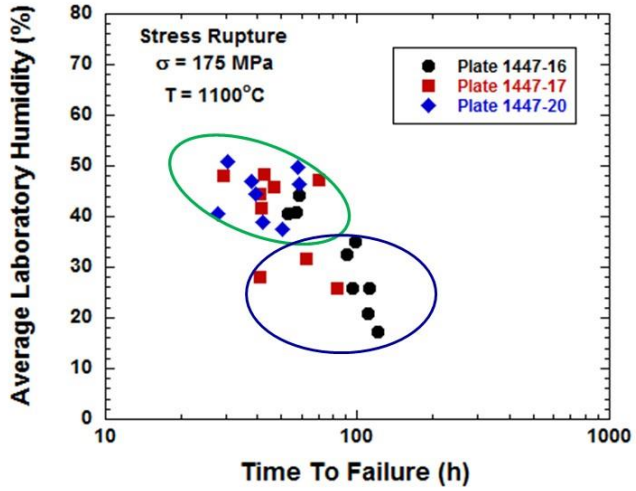

Figure 38. Humidity Versus Log Time to Failure Showing Two Groups of Data

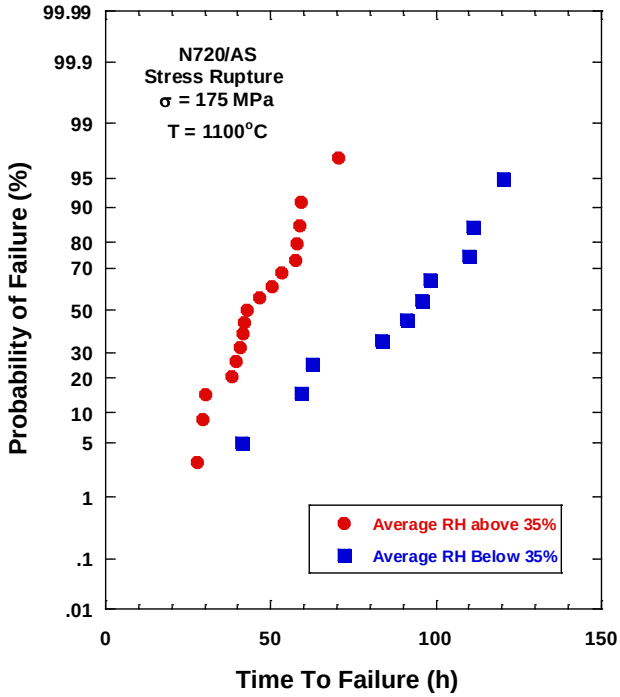

Figure 39. POF Plot for N720/AS for Average Humidity Above and Below 35%

DISTRIBUTION STATEMENT A. Approved for public release: distribution is unlimited.
88ABW-2019-2847

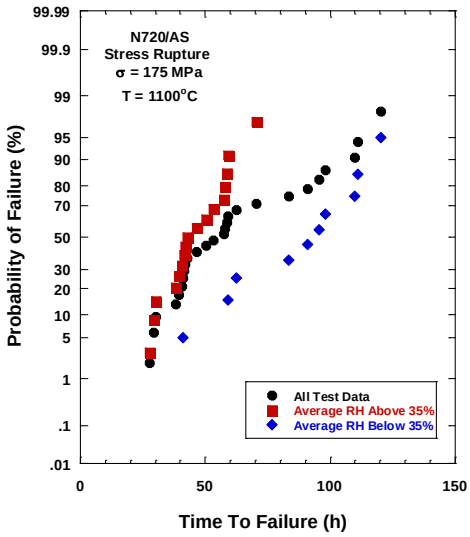

Figure 40. POF Plot Comparing Entire Data Set To Humidity Data Sets

6.4 Failure Location for Each Test Specimen

ASTM requires the measurement of the failure location after each test. These measurements were made and are presented in **Error! Reference source not found.**. It was observed that failure tended to occur near or at the transition between the straight gage section and the radius of the dogbone test specimen. Location of failure is better observed in a plot of failure location versus time to failure, as shown in Figure 41, along with a drawing of the test specimen to help illustrate where failure occurred. In this case, the failure location is the distance measured from the load cell end of the specimen (left end). Several important observations can be made from this figure. The plot illustrates that, with the exception of a few specimens, the most failures occurred at the transition region of the dogbone radius. What is encouraging is that the failures appear to be randomly distributed at both the left and right radii. This is attributed to the high degree of alignment, as well as the excellent thermal profile, which may also have unexpectedly contributed to the failures occurring at the radius.

Oxide/Oxide CMCs will generally fail at the hottest location during stress rupture testing. However, for these tests, the thermal profile produced less than 1% variation in temperature along the gage length of the specimen, and the profile was extremely flat out past the two radii. As shown earlier with the microscopy, the microstructure of this N720/AS material is very uniform with no significant defects. The data suggests that any defects in the material are significantly smaller than the damage that occurs at the radius. In studying the data, there appears to be no real effect on the rupture life compared to those specimens that failed in the machined gage section. Figure 42 is an optical photograph of a specimen that failed near the center of the gage section and lasted only ~70 hours, while Figure 43 is a photograph of a specimen that failed right at the radius, even though it lasted ~111 hours. However, it is apparent that damage at the radius did influence the test results and should be considered censored test data. It is acknowledged that the lifetimes measured are actually a lower conservative bound and that, without the damage occurring at the radius, the lives may have been longer. Therefore, the test data should be treated as right-censored data.

DISTRIBUTION STATEMENT A. Approved for public release: distribution is unlimited.
88ABW-2019-2847

Table 9. Location of Failure for N720/AS Stress Rupture Specimens

Sample (ID)	Average From Left End (mm)	Distance From Cenerline (mm)	Description Of Fracture
11-736	103	14	slope through gage
11-737	103	14	alternating steps within thickness
11-738	72	-17	sloped step
11-739	75	-14	flat
11-740	79	-10	step
11-741	75	-14	flat
11-743	75	-14	sloped step
11-744	107	18	flat
11-745	78	-11	sloped step
11-746	105	16	flat with spiking
11-747	91	2	flat with spiking
11-748	107	18	flat
11-749	75	-14	flat with spiking
11-750	105	16	flat with spiking
11-751	73	-16	flat
11-753	89	0	flat
11-754	73	-16	flat
11-755	73	-16	flat with spiking
11-756	75	-14	sloped step
11-757	75	-14	flat with spiking
11-780	73	-16	flat with spiking
11-781	72	-17	flat
11-782	89	0	step
11-783	72	-17	flat
11-784	73	-16	slope through gage
11-787	75	-14	flat
11-788	101	12	flat
11-789	100	11	flat
11-790	102	13	flat
Tension Tests At 1100°C			
11-742	80	-9	step
11-752	80	-9	step
11-785	75	-14	Very stepped over 25 mm in length

Note: Distance From Center: Negative Left of Cener, Positive Right Of Center
Note: Gage Length 28 mm

DISTRIBUTION STATEMENT A. Approved for public release: distribution is unlimited.
88ABW-2019-2847

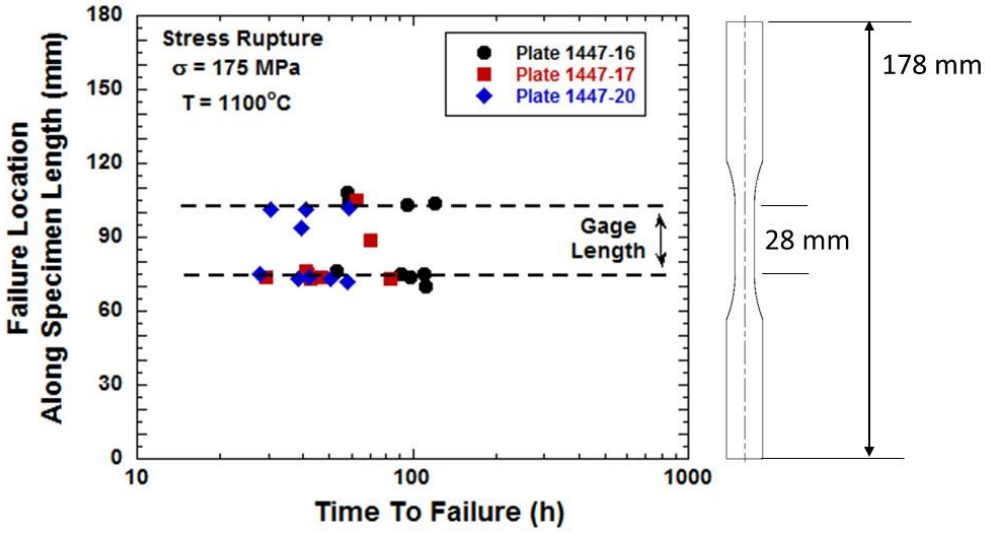

Figure 41. Failure Location Versus Time to Failure for N720/AS Stress Rupture Tested at 175 MPa And 1100°C

Figure 42. Photograph of Failed Stress Rupture Specimen That Ran ~70 Hours

Figure 43. Photograph of Failed Stress Rupture Specimen That Ran ~111 Hours

6.5 Test Specimen Dimensions

The ASTM round-robin for tension testing did a nice job of documenting the variability in the measurements of width and thickness of the test specimens. Slight differences were observed between the nine different laboratories, as well as the type of micrometer used to make the measurements. The ASTM study found a variation in thickness measurement, with the thickness mean being 2.77 mm and a standard deviation of 0.07 mm. This produced a coefficient of variation of 2.5%. For this study (see **Error! Reference source not found.**), the mean thickness was 2.692 mm with a standard deviation of only 0.033 mm, and a coefficient of variation of only 1.22%. This data highlights that the N720/AS panels were manufactured very uniformly. A plot of specimen thickness versus time to failure is presented in Figure 44. There appears to be a very slight dependence of rupture life on thickness; however, the fit parameter is very low.

It is suggested that the observed behavior of thinner specimens exhibiting longer rupture lives might be explained as follows. Each of the panels was manufactured with 12 plies and the fiber volume fraction is very uniform. Therefore, during the autoclave cycle, one side of the panel is against a flat hard tool, while the other is against the bagging material. As the panels compress, some regions might compress slightly more than others because of the use of the bagging

DISTRIBUTION STATEMENT A. Approved for public release: distribution is unlimited.
88ABW-2019-2847

material. If a rigid panel was used on both sides with specific hard stops, then the panel thicknesses would have been much more uniform. In oxide/oxide CMCs, the fibers carry all the load during static loading and the very porous matrix does not significantly contribute to the load-carrying capability. Therefore, a slightly thinner specimen with the same amount of fibers would be at a lower load level to achieve the same stress. This slightly lower load level would be expected to result in longer stress rupture lives, and is the trend shown in Figure 44. The same data can also be presented as applied load versus time to failure, as shown in Figure 45, and also exhibits a very low fit parameter.

Another point of consideration when studying the results is that variability in the measurement of the specimen dimensions affects the test loads. From the ASTM study, thickness showed the most variation. Therefore, a table of the seven thickness measurements taken along the gage length of each specimen and grouped by panel is presented in **Error! Reference source not found.**. Here, it appears that the panels are very uniform with very little variation, an example being the coefficient of variation that are all within 1.043% to 1.39%. The average thickness values can also be presented graphically, as shown in Figure 46. Panel 1447-16 varied by 4 microns while Panels 1447-17 and 1447-20 both varied by 12 microns.

The data also supports that there was no thickness variation at either radius location in the test specimens. Width measurements were also carefully checked and there was no undercutting of the radius or uneven machining of the widths. This data supports the earlier suggestion that the high percentage of failures located at the radius were the result of damage occurring at the transition region of the radius and not the test specimen dimension.

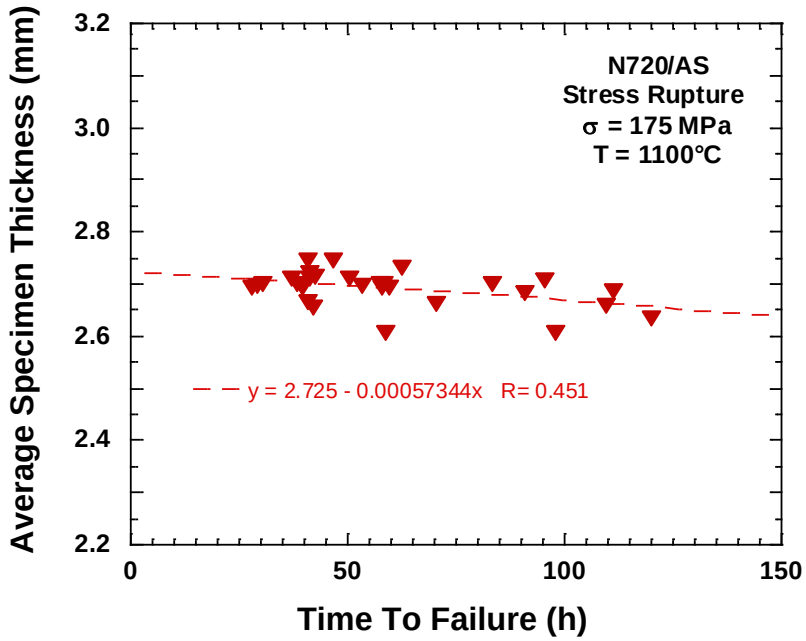

Figure 44. Average Specimen Thickness Versus Rupture Time for N720/AS

DISTRIBUTION STATEMENT A. Approved for public release: distribution is unlimited.
88ABW-2019-2847

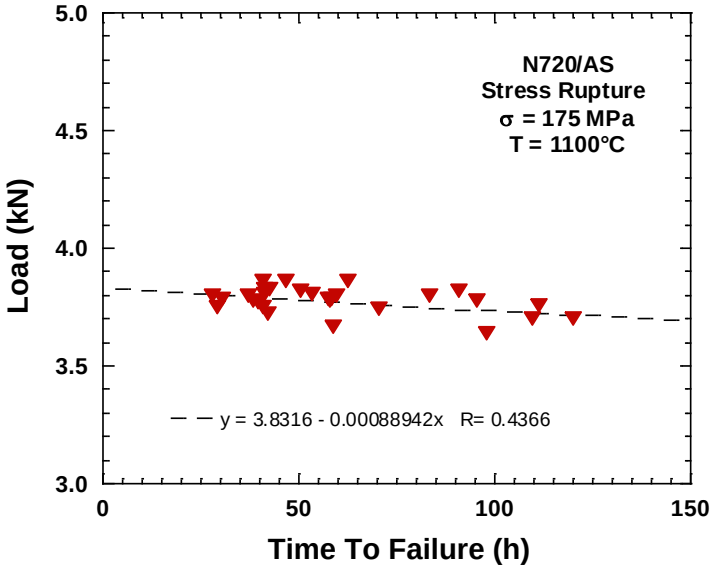

Figure 45. Applied Load Versus Rupture Time for N720/AS

DISTRIBUTION STATEMENT A. Approved for public release: distribution is unlimited.
88ABW-2019-2847

Table 10. Thickness of Test Specimens Along Gage Length

Panel ID From COIC	Air Force Specimen ID	Thickness -13.85 mm From CL (mm)	Thickness -9.23 mm From CL (mm)	Thickness -4.62 mm From CL (mm)	Thickness 0 CL (mm)	Thickness 4.62 mm From CL (mm)	Thickness 9.23 mm From CL (mm)	Thickness 13.85 mm From CL (mm)
1447-16	11-736	2.620	2.628	2.646	2.628	2.643	2.648	2.639
1447-16	11-737	2.713	2.709	2.704	2.71	2.701	2.705	2.703
1447-16	11-738	2.691	2.684	2.684	2.691	2.690	2.678	2.689
1447-16	11-739	2.664	2.658	2.655	2.664	2.668	2.650	2.661
1447-16	11-740	2.604	2.606	2.605	2.612	2.606	2.604	2.613
1447-16	11-741	2.693	2.681	2.679	2.672	2.692	2.687	2.673
1447-16	11-742	2.696	2.697	2.684	2.695	2.695	2.695	2.689
1447-16	11-743	2.701	2.697	2.696	2.698	2.692	2.696	2.702
1447-16	11-744	2.707	2.713	2.709	2.704	2.698	2.693	2.693
1447-16	11-745	2.711	2.717	2.717	2.716	2.703	2.708	2.707
1447-16	11-746	2.696	2.696	2.709	2.714	2.698	2.700	2.681
Average		2.681	2.681	2.681	2.682	2.681	2.679	2.677
Standard Deviation		0.035	0.034	0.032	0.033	0.029	0.030	0.028
Coefficient of Variation (%)		1.313	1.273	1.196	1.241	1.080	1.136	1.043
1447-17	11-747	2.683	2.667	2.689	2.707	2.703	2.703	2.691
1447-17	11-748	2.687	2.697	2.703	2.707	2.709	2.700	2.712
1447-17	11-749	2.706	2.712	2.702	2.708	2.711	2.717	2.709
1447-17	11-750	2.706	2.738	2.742	2.738	2.732	2.740	2.737
1447-17	11-751	2.744	2.749	2.747	2.751	2.751	2.748	2.741
1447-17	11-752	2.616	2.618	2.619	2.616	2.614	2.621	2.628
1447-17	11-753	2.653	2.656	2.668	2.661	2.665	2.665	2.674
1447-17	11-754	2.709	2.695	2.697	2.698	2.705	2.686	2.692
1447-17	11-755	2.706	2.712	2.712	2.709	2.708	2.720	2.724
1447-17	11-756	2.726	2.736	2.744	2.748	2.751	2.754	2.759
1447-17	11-757	2.716	2.717	2.715	2.727	2.726	2.722	2.723
Average		2.696	2.700	2.703	2.706	2.707	2.707	2.708
Standard Deviation		0.034	0.038	0.036	0.037	0.037	0.037	0.035
Coefficient of Variation (%)		1.254	1.390	1.314	1.385	1.378	1.370	1.276
1447-20	11-780	2.648	2.647	2.655	2.659	2.656	2.666	2.660
1447-20	11-781	2.684	2.686	2.694	2.688	2.694	2.700	2.699
1447-20	11-782	2.671	2.683	2.698	2.699	2.705	2.702	2.708
1447-20	11-783	2.699	2.699	2.707	2.710	2.722	2.719	2.723
1447-20	11-784	2.704	2.713	2.713	2.703	2.693	2.692	2.689
1447-20	11-785	2.720	2.720	2.713	2.722	2.735	2.727	2.731
1447-20	11-786	2.715	2.718	2.720	2.721	2.715	2.717	2.714
1447-20	11-787	2.687	2.682	2.691	2.693	2.691	2.697	2.703
1447-20	11-788	2.693	2.700	2.700	2.708	2.707	2.702	2.698
1447-20	11-789	2.657	2.669	2.668	2.666	2.657	2.666	2.670
1447-20	11-790	2.604	2.601	2.609	2.609	2.609	2.610	2.612
Average		2.680	2.683	2.688	2.689	2.689	2.691	2.692
Standard Deviation		0.032	0.033	0.031	0.032	0.034	0.032	0.032
Coefficient of Variation (%)		1.201	1.244	1.158	1.179	1.279	1.171	1.193

DISTRIBUTION STATEMENT A. Approved for public release: distribution is unlimited.
88ABW-2019-2847

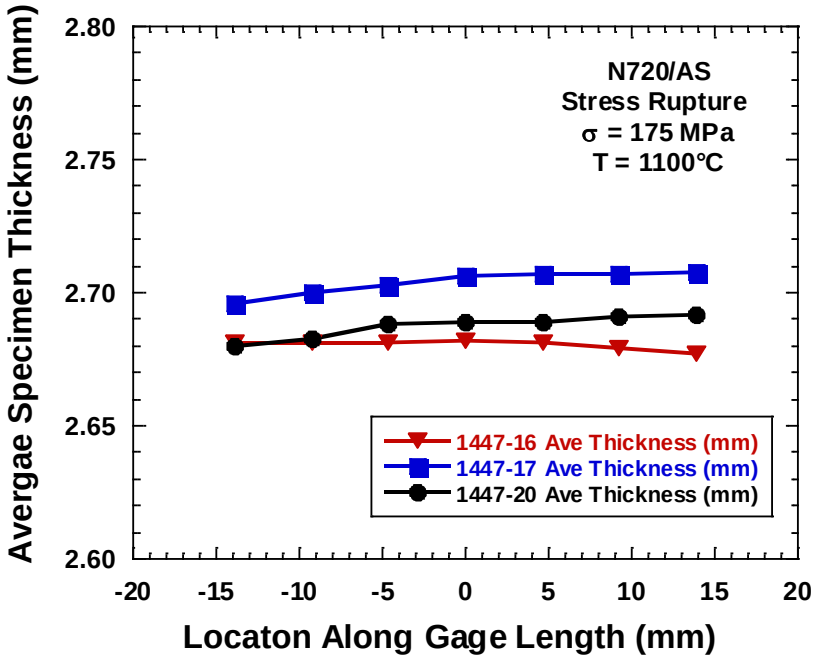

Figure 46. Average Test Specimen Thickness Along Length of Specimens

6.6 Test Specimen Design

The test specimen design used in this study is often used by AFRL/RXCCP for many CMCs. These non-oxide CMC systems often experience ITE, which can cause these non-oxide CMCs to fail outside of the heated gage section during elevated-temperature tests. These failures occur more often for longer term tests and also occur more frequently when cool grips are used. This ITE failure location is driven when the center hot section of the specimen is at maximum temperature and is somewhat protected from oxidation by sealing phases. In contrast, the material outside the hot zone does not experience any sealing, but carbon and born nitride can still oxidize. The occurrence of ITE becomes more prevalent as the stress level is decreased and test time increases. Therefore, the shorter the gage length and the smaller the radius, the less likely an ITE failure will occur, because the specimen will be much wider where the temperature starts to decrease. The tradeoff is that decreasing the radius increases the stress concentration that is generated at the start of the transition region of the radius. ITE was not a concern for the oxide/oxide CMC system tested in this study.

In Table 9, the location of each failure was presented for the 29 stress rupture experiments conducted on N720/AS. A total of 12 test specimens failed outside the machined gage length of 28 mm, nine failed essentially right at the radius, and eight failed inside the machined gage section. Per the ASTM standard, 41% of the test specimen failures were outside of the machined gage section and, therefore, need to be considered as right-censored test data.

In order to address this, a straightforward plane stress analysis was performed on the test specimen used in this investigation. This assumed linear elastic material behavior with homogenous isotropic properties incorporating an elastic modulus of 70 GPa and Poisson's ratio

DISTRIBUTION STATEMENT A. Approved for public release: distribution is unlimited.
88ABW-2019-2847

of 0.12. A script was developed to automate the analysis which read an input file with the specimen dimensions and then created the model geometry, meshed the region and set all boundary conditions and loads. The user manually ran the analysis and extracted desired results. A simple mesh refinement study was completed to show that the mesh size accurately captured the stress gradient near the stress concentration factor (Kt) for each geometry. The stress concentration factor for the specimen geometry used in this investigation was calculated by dividing the maximum axial stress by the nominal axial stress in the specimen gage section ($Kt = \sigma max/\sigma net$). The stress analysis showed that the specimen geometry had a stress concentration factor of 1.044, and this maximum stress concentration occurred approximately 1 mm outside of the uniform gage section. A total of 16 specimens failed within ±1 mm of this location and 20 failed within ±2 mm.

A stress contour plot for the standard test specimen for an applied stress of 100 MPa net section stress is shown in Figure 47. A ±2% variation is shown, and one can observe that the maximum stress concentration actually occurs slightly away from the very beginning of the transition region. A plot showing how stress varied along the length of the standard test specimen is presented in Figure 48, with the red line representing the beginning of the radius. As previously stated, stress maximized approximately 1 mm beyond the start of the radius.

Several additional established test specimen geometries were analyzed using the same procedure to investigate this further. The exact specimen dimensions and corresponding stress concentration values are presented in **Error! Reference source not found.**, and range from a high of 1.079 to a low of 1.007.
Several of the specimen designs have a K_t under 1%. Therefore, an attempt was made to select an optimized specimen design that would reduce the K_t while also meeting the following testing requirements. The gage width was to be at least 8 mm wide to account for 8HSW fiber architectures, and the gage length was to be kept at 28 mm to allow for 25.4 mm extensometers. In addition, the reduction in area was to 35% or larger to accommodate test specimens with UTS above 300 MPa, and the length was to remain at 178 mm to accommodate current furnace configurations. Variation in thickness for the N720/AS material was found to be slightly larger than 1%. Therefore, the stress concentration needed to be less than this 1% variation.

Using this criteria, a specimen was identified as meeting all these requirements, and is shown in a schematic in Figure 49. It has a length of 178 mm, width of 15 mm, gage length of 28 mm, gage width of 8 mm, and radius of 317mm. This geometry results in a stress concentration that is only 1.007. A stress contour plot was generated for this new geometry and is presented in Figure 50, where it is easy to see how the stress concentration has been significantly reduced from that shown for the standard specimen in Figure 47 .

The details of the stress concentrations for both geometries can be addressed by plotting the stress that occurs from the center to the edge of the specimen. The stress profile across the width at the end of the uniform gage section is presented in Figure 51 It is clear that, directly at the radius, the stress for the standard geometry is already 2% higher than in the gage section. As stated earlier, the maximum stress occurs approximately 1 mm outside of the gage section. A stress profile across the width at the location of maximum stress is presented in Figure 52. In

DISTRIBUTION STATEMENT A. Approved for public release: distribution is unlimited.
88ABW-2019-2847

this figure, the stress for the standard geometry is 4% above that in the gage section, while the new geometry is below 1%. This new geometry meets all of the testing parameters.

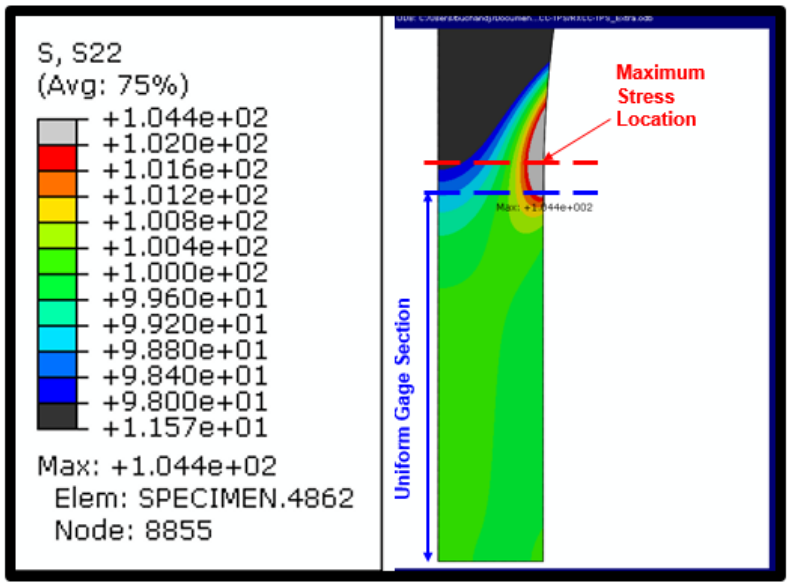

Figure 47. Stress Contour Plot with ±2% Variation from Applied 100 MPa Net Section Stress for Standard Test Specimen

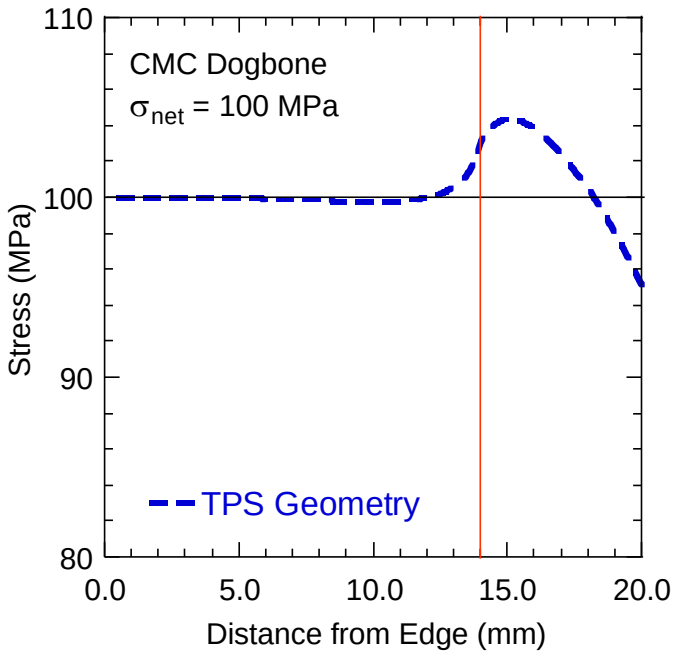

Figure 48. Maximum Localized Stress Value Along Length of Standard Test Specimen

DISTRIBUTION STATEMENT A. Approved for public release: distribution is unlimited.
88ABW-2019-2847

Table 11. Stress Concentration Factors for Several Different CMC Dogbone-Shaped Specimens

Specimen Geometry	Specimen Dimensions					Stress Concentration Factor
	Specimen Length L (mm)	Specimen Width W (mm)	Gage Length GL (mm)	Gage Width GW (mm)	Transition Radius R(mm)	Kt,net
Variability: Original (AFRL/RXCC)	178	15	28	8	50	1.044
Variability: New (AFRL/RXCC)	178	15	28	8	317	1.007
ASTM C1275 Tension Test	200	10	40	8	30	1.079
SNECMA Test Specimen	120	24	30	10	60	1.045
ASTM C1275 Tension Test	152	25.4	30.48	5.287	76.2	1.019
ASTM C1275 Tension Test	175	12	36	6	100	1.017
Thesis (Dan Dunn)	152	13	38	10	178	1.016
ASTM C1275 Tension Test	111.7	14	33	6.3	152.4	1.012
Enabeling Propulsion Materials	152	12.7	15.24	10.16	368	1.008
TTCP (AFRL/RXCC)	152	12.8	27.94	8	305	1.007

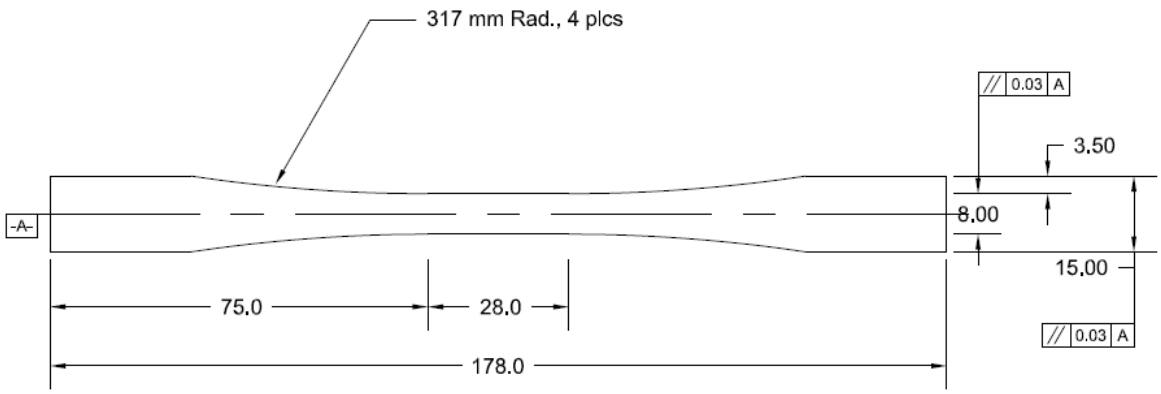

Figure 49. Schematic of New Dogbone Test Specimen Geometry for Future Variability Studies

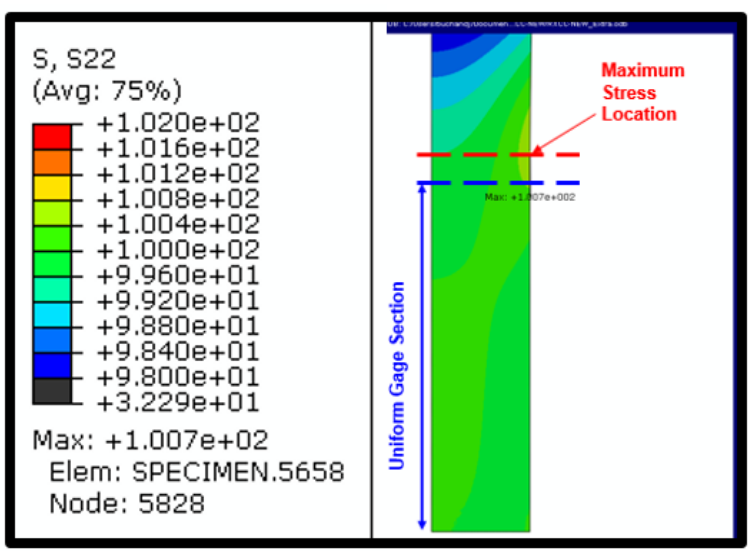

Figure 50. Stress Contour Plot with ±2% Variation from Applied 100 MPa Net Section Stress for Revised Test Specimen

DISTRIBUTION STATEMENT A. Approved for public release: distribution is unlimited.
88ABW-2019-2847

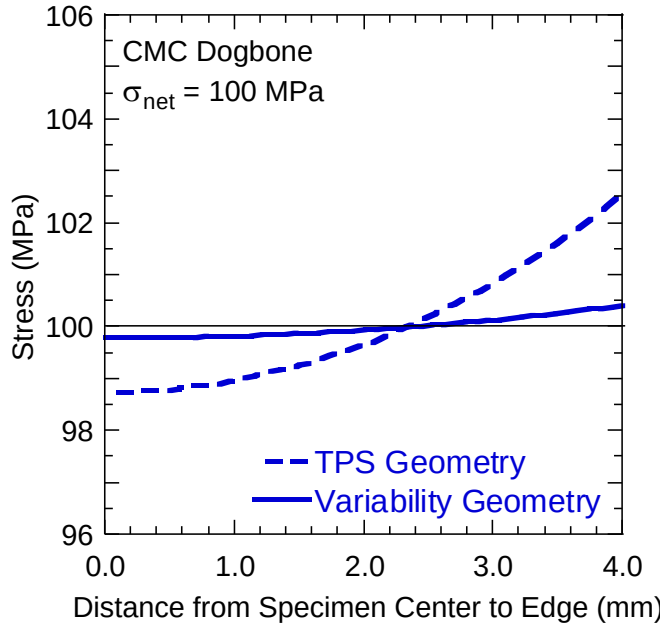

Figure 51. Stress Versus Distance from Specimen Center to Edge at End of Uniform Gage Section

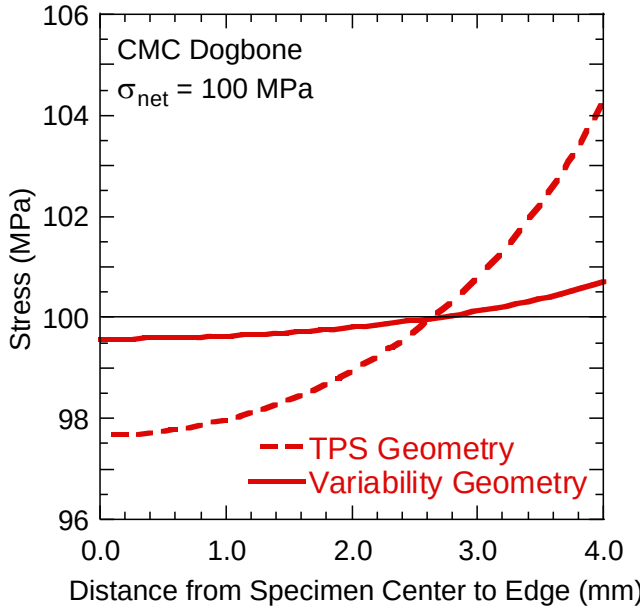

Figure 52. Stress Versus Distance from Specimen Center to Edge at Location of Maximum Stress (29 mm from Center)

6.7 Effect of Cut Fibers at the Radius

As discussed earlier, the use of a dogbone specimen is necessary when testing CMCs to greatly reduce the chance of failure occurring at the grips. This is especially true for tension tests, but dogbone test specimens may not be necessary for stress rupture testing where the applied stress levels are often well below the tensile strength of the CMCs. The presence of the machined

DISTRIBUTION STATEMENT A. Approved for public release: distribution is unlimited.
88ABW-2019-2847

radius creates two important issues associated with how damage initiates in the test specimen. The first has to do with the stress concentration factor that was addressed above. In addition, the introduction of the radius also results in cut fibers and fiber tows at the transition point from the gage section to the radius. Improvements to damage models has pointed to issues associated with the cut fiber tows immediately next to the continuous fiber tows that span the gage section. These first cut fiber tows that are exposed to the free surface of the transition region are subjected to a stress state that results in shear damage along the fiber tow. It is postulated that this shear damage to the matrix at this location results in local matrix damage leading to a localized weakness in the matrix. It is this localizing damage that triggers the initiation of the failure process. These oxide/oxide CMCs do not have an engineered fiber/matrix interface, and have relatively strong bonding between the fibers and the matrix. It is speculated that the degradation of the local matrix strength is coupled with high interface forces ultimately leads to through-thickness matrix failure in the transition zone of the test specimen.

This postulation could be studied by testing in stress rupture specimens with stress concentration values of 1.044 and 1.007, and then comparing those results to straight sided specimens. The stress concentration of 1.04 would combine a high stress concentration with cut fiber tows, whereas the lower stress concentration would be below the scatter in thickness measurement while still having cut fiber tows at the transition region. The straight sided specimens would have no cut fibers and no stress concentration. This should work well for oxide/oxide CMCs that do not exhibit ITE.

DISTRIBUTION STATEMENT A. Approved for public release: distribution is unlimited.
88ABW-2019-2847

7. CONCLUSIONS AND RECOMMENDATIONS

A series of stress rupture experiments on N720/AS conducted at a stress of 175 MPa and temperature of 1100°C revealed several important findings. The scatter in the measured lifetimes was found to be less than one order of magnitude.

The test machine was very well aligned to approximately 2% bending at 500 micro-strain.

The temperature along the length of the test specimen was thoroughly documented and the temperature profile along the length of the gage section varied by less than 1% from the test temperature of 1100°C.

Failures were often located at, or just outside, of the radius of the dogbone test specimen. A total of 12 test specimens failed outside the machined gage length of 28 mm, nine failed directly at the radius, and only eight failed inside the machined gage section. Per the ASTM standard, 41% of the test specimen failures were outside of the machined gage section and, therefore, need to be treated as right-censored test data.

POF plots identify that one of the three panels produced for this study exhibited significantly longer lives. Detailed studies identified that relative humidity in the laboratory may have been the cause. Those specimens tested at low relative humidity exhibited much longer lives than those tested during periods of higher humidity. Probability plots were compared for specimens tested when relative humidity was above and below 35%, which documented that relative humidity was, indeed, influencing stress rupture life.

Detailed analysis of the test specimen dimension supports that there was no thickness variation issue at either radius locations. Width measurements were also carefully checked and there was no undercutting of the radius or uneven machining of the widths. This data supports the suggestion that the high percentage of failures located at the radius were the result of the stress concentration and not an issue with the test specimen dimension.

A new test specimen was designed that meets test equipment requirements while reducing the stress concentration from 1.044 down to 1.007. This new geometry should work well for oxide/oxide CMCs. However, other CMCs such as PIP-manufactured SiC/SiC or C/SiC that exhibit ITE may require a different geometry.

It is suggested that the stress concentration, in addition to the presence of cut fiber tows at the transition region of the radius, drive the failure location. Therefore, it is suggested that future creep rupture studies investigate two specimen geometries with different Kt (1.04 and 1.07), and a straight sided specimen geometry. Such a series of experiments should identify if it is the stress concentration, or the presence of cut fiber tows, that drives failure location.

It is recommended that a humidity chamber be used to stabilize relative humidity to one level for the entire test series.

DISTRIBUTION STATEMENT A. Approved for public release: distribution is unlimited.
88ABW-2019-2847

8. REFERENCES

[1] R. John, D.J. Buchanan, and L.P. Zawada, "Creep Deformation and Rupture Behavior of a Notched Oxide/Oxide Nextel720/AS Composite," in 24th Annual Conference on Composites, Advanced Ceramics, Materials, and Structures: A: Ceramic Engineering and Science Proceedings, Volume 21, Issue 3 (eds., T. Jessen and E. Ustundag), John Wiley & Sons, Inc., Hoboken, NJ, USA (2000).

[2] S.T. Gonczy, "Tensile Testing of Nicalon 2-D Fiber-Reinforced Sylramic S-200 Ceramic Composites – A Multi-Laboratory Round-Robin Test," Gateways Materials Technology Report #TR99-1, April, 1999.

[3] Reynaud, P., "Cyclic Fatigue of Ceramic-Matrix Composites at Ambient and Elevated Temperatures," Composites Science & Technology, Volume 56, PP. 809-814, 1996.

[4] ASTM E1012-14, "Standard Practice for Verification of Testing Frame and Specimen Alignment Under Tensile and Compressive Axial Force Application," ASTM, 100 Barr Harbor Drive, West Conshohocken, PA, USA, July 21, 2014

[5] Zawada, K. Davidson, and J. Pierce, ", "Configuration and Calibration of High Temperature Furnaces for Testing Ceramic Matrix Composites," AFRL-RX-WP-TR-2014-0168.

[6] ASTM C1275-00, "Standard Test Method for Monotonic Tensile Behavior of Continuous Fiber-Reinforced Advanced Ceramics with Solid Rectangular Cross-Section Test Specimens at Ambient Temperatures," ASTM, 100 Barr Harbor Drive, West Conshohocken, PA, USA, June 10, 2000

[7] ASTM C1275-00, Standard Test Method for Monotonic Tensile Behavior of Continuous Fiber-Reinforced Advanced Ceramics with Solid Rectangular Cross-Section Test Specimens at Ambient Temperatures, ASTM, 100 Barr Harbor Drive, West Conshohocken, PA, USA, June 10, 2000.

[8] ASTM C1337-96, "Standard Test Method for Creep and Creep Rupture of Continuous Fiber-Reinforced Advance Ceramics with Solid Rectangular Cross-Section Test Specimens at Elevated Temperatures," June 10, 1996, ASTM, 100 Barr Harbor Drive, West Conshohocken, PA. USA

DISTRIBUTION STATEMENT A. Approved for public release: distribution is unlimited.
88ABW-2019-2847

LIST OF SYMBOLS, ABBREVIATIONS, AND ACRONYMS

8HSW	eight-harness satin weave
AFRL/RXCC	Composites Branch, Structural Materials Division of the Materials & Manufacturing Directorate, Air Force Research Laboratory
AS	alumino-silicate
ASTM	American Society for Testing and Materials
C/C	carbon/carbon
CMC	ceramic matrix composite
COIC	COI Ceramics, Incorporated.
E	modulus
ε_f	strain at failure
ITE	intermediate temperature embrittlement
M&P	Materials & Processing
MATE	material analysis and testing
MTS	MTS Systems Corporation
PIP	polymer infiltration and pyrolysis
PL	proportional limit
POF	probability of failure
RH	relative humidity
SEM	scanning electron microscope
SiC	silicon carbide
TC	thermocouple
UDRI	University of Dayton Research Institute
USAF	United States Air Force
UTC	United Technology Corporation
UTS	ultimate tensile strength
WPAFB	Wright Patterson Air Force Base

DISTRIBUTION STATEMENT A. Approved for public release: distribution is unlimited.
88ABW-2019-2847